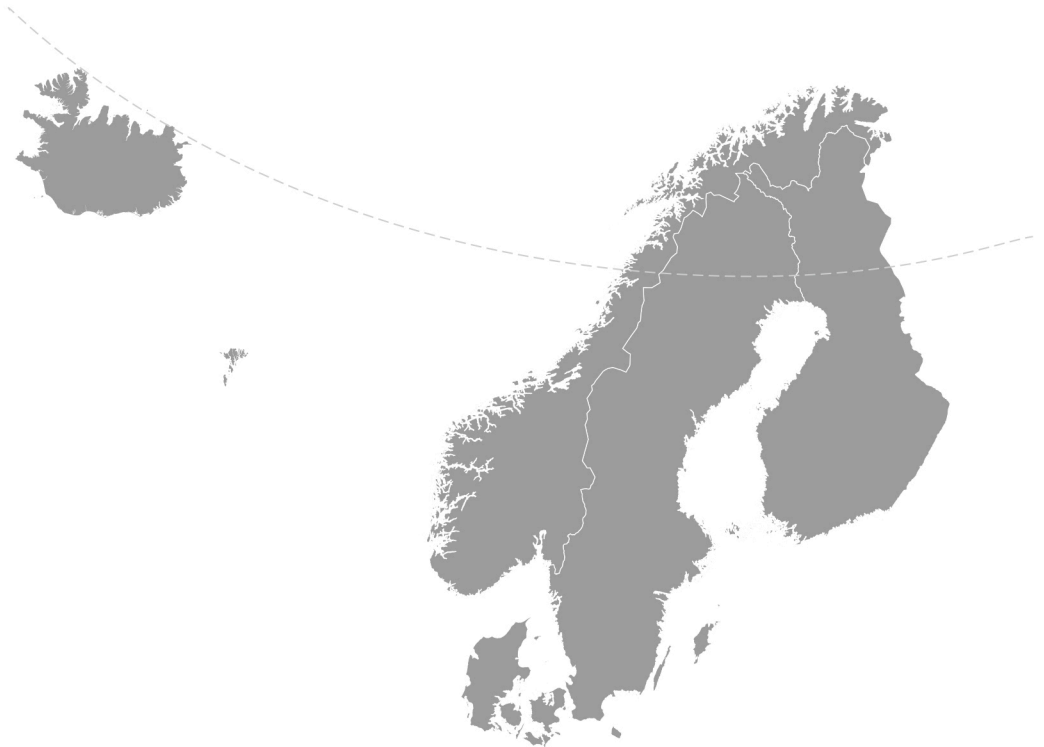


Nordic Concrete Research



Nordic
Concrete
Federation

PUBLICATION NO. 46 2/2012

NORDIC CONCRETE RESEARCH

**EDITED BY
THE NORDIC CONCRETE FEDERATION**

**CONCRETE ASSOCIATIONS OF: DENMARK
FINLAND
ICELAND
NORWAY
SWEDEN**

**PUBLISHER: NORSK BETONGFORENING
POSTBOKS 2312, SOLLI
N - 0201 OSLO
NORWAY**

VODSKOV, DECEMBER 2012

Preface

Nordic Concrete Research is since 1982 the leading scientific journal concerning concrete research in the five Nordic countries, e.g., Denmark, Finland, Iceland, Norway and Sweden. The content of *Nordic Concrete Research* reflects the major trends in the concrete research.

Nordic Concrete Research is published by the Nordic Concrete Federation that beside the publication activity also organizes the Nordic Concrete Research Symposia that have constituted a continuous series since 1953 in Stockholm. The Symposium circulates between the five countries and takes normally place every third year. The next symposium, no. XXII, will be held Reykjavik, Iceland **13 - 15 August 2014**, in parallel with the ECO-CRETE conference. (The symposium have formerly been announced to be held 19 - 21 June 2013)

Since 1982, 391 papers have been published in the journal. Since 1994 the abstracts and from 1998 both the abstracts and the full papers can be found on the Nordic Concrete Federation's homepage: www.nordicconcrete.org. The journal thus contributes to dissemination of Nordic concrete research, both within the Nordic countries and internationally. We are very pleased, that during the latest years, growing interests in participating in the Nordic Concrete Research symposia, as well as for publishing in NCR have been observed.

Since 1975, 75 Nordic Miniseminars have been held – it is the experience of the Research Council of the Nordic Concrete Federation, that these Miniseminars have a marked influence on concrete research in the Nordic countries. In some cases, the information gathered during such Miniseminars has been used as Nordic input to CEN activities.

Vodskov, December 2012

Dirch H. Bager

Editor, *Nordic Concrete Research*

CONTENTS

1	Rolands Cepurītis Yield stress and slump-flow of SCC: Short review and application	1
2	Majid Al-Gburi, Jan-Erik Jonasson, Martin Nilsson, Hans Hedlund & Anders Hösthagen Simplified Methods for Crack Risk Analyses of Early Age Concrete Part 1: Development of Equivalent Restraint Method	17
3	Majid Al-Gburi, Jan-Erik Jonasson, S. T. Yousif & Martin Nilsson Simplified Methods for Crack Risk Analyses of Early Age Concrete Part 2: Restraint Factors for Typical Case Wall-on-Slab	39
4	Jonny Nilimaa, Thomas Blanksvärd, Lennart Elfgren & Björn Täljsten Transversal Post Tensioning of RC Trough Bridges – Laboratory Tests	57
5	Mikael Hallgren Nordic Workshop on Finite Element Analysis of Concrete Structures	75
	Research Council and Editorial Board of NCR	79
	Review Group	81

Yield stress and slump-flow of SCC: Short review and application



Rolands Cepurītis
 B.Sc. Eng., M.Sc. Eng, PhD Candidate
 Norcem AS, R&D Department
 c/o NTNU, Department of Structural Engineering
 Richard Birkelands vei 1A,
 NO-7491 Trondheim
 E-mail: rolands.cepuritis@norcem.no

ABSTRACT

In this paper a short review on the relevant previous work is given and the applicability of an existing analytical model to evaluate yield stress τ_0 from spread measurements of cementitious suspensions is verified for self-compacting concrete (SCC). Based on limited amount of results included in this work, it is possible to demonstrate the potential of the given model to be used in order to evaluate yield value of a SCC mix from spread measurements performed with a standard slump cone. The model seems to be applicable for mixes with a slump-flow higher than 550 mm, i.e. for the complete SCC range.

Key words: Fresh concrete, self-compacting concrete, SCC, rheology, workability, slump-flow, yield stress.

1. INTRODUCTION AND BACKGROUND

1.1. Current status of SCC application

Self-Compacting Concrete (SCC) can't be considered a new material anymore since it has been invented or more precisely defined already in 1988 by prof. Okamura and his students Ozawa and Maekawa (Okamura and Ouchi, 1988 as cited in [1]). Even though replacement of Conventional Vibrated Concrete (CVC) by SCC generally introduces a wide range of immediate benefits such as reduction of labour costs, quicker casting, allows much denser reinforcement, better quality of the structure etc., there are also some drawbacks. The most unwanted consequences usually being increased formwork pressure, reduced robustness of the mix and cost of the material per m³. A lot of efforts have lately been put in order to reduce the cost of SCC (like the ECO-SCC concept by Wallevik [2]) and to prove that benefits from the use of SCC in a lot of cases can overcome the drawbacks [3-4]. However, experience of the author shows that at least in the Baltic market contractors are still quite sceptical. The reason usually being just a narrow look at the material price per m³ instead of getting the "big picture" and trying to estimate the total costs. Or in different words, the contractors usually inquire about the price and don't want to look into more details when they find out that it can be reasonably higher than for CVC. Lack of knowledge in handling SCC projects and some negative previous experience with formwork failure in some cases is also a reason why the application of SCC is still rather limited. As a consequence, in most of the developed countries the market share of

SCC is only a couple of % from the total ready-mix production [5]. A good example in this case is Denmark where the share of SCC can reach up to 1/3 of annual ready mix concrete production [1, 5]. However, it must also be noted that in Denmark SCC with comparably high yield value of around 60 Pa or slump-flow around 550 mm (called also the “high-yield SCC”) is usually used [1]. Naturally, very low plastic viscosity (20 Pa·s or even lower), is required in order to use the concrete with no external vibration [1]. Some unpublished discussions have revealed that if the Danish definition of SCC is applied, the market share in countries like Norway can be even higher than 1/3 as it is claimed to be in Denmark.

1.2. Technology transfer from CVC to SCC

The older and as described in the previous section also much more popular brother of SCC is CVC which has been around already from 1824 when a bricklayer and builder from England James Aspdin patented Portland cement [6]. During the years many generations of concrete contractors, producers and researchers have been around while CVC stayed in general terms the same until the introduction of superplasticizers. Especially so-called 3rd generation (polycarboxylate based) superplasticizers or “ π -polymers” that were first used during the 1980’s [7]. Invention of the later was probably the biggest step forward in the direction of SCC development. However, some part of the existing concrete technology and knowledge on the topic available is still applicable only for the CVC, even though the two are sometimes very similar in properties and composition. This is usually true in case of very flowable (slump > 230 mm) and moderate or high strength CVC (with high cement or fines content). Like the Particle-Matrix (P-M) model for proportioning that regards all particles > 0.125 mm as a particle phase dispersed in a lubricating matrix made up of all fluids (water, admixtures etc.) and particles (binder, filler etc.) < 0.125mm. Having determined the properties of each phase, the concrete workability is defined as a unique function of the volume relations between the two [8]. The method has been used in Scandinavian countries (especially Norway) by many practitioners for more than a decade and has proven to be very useful. It was initially developed to proportion CVC but in case of SCC the workability function seems to be affected by some other not so well defined parameters of the used mineral fines (like grading, specific surface, moisture adsorption, admixture adsorption, shape, packing, z-potential etc.). This means that with the existing knowledge the P-M model workability function approach it is not so successfully if at all applicable for very flowable concrete (personal communication with E. Mørtzell). So in some cases it is very essential to verify if a model of an approach developed is also applicable for concrete with very high flowability and SCC.

1.3. Concrete workability description possibilities

In 1983 Tattersall and Banfill proposed the Bingham model (Equation (1)) to be used in order to approximate workability of fresh concrete over practical shear rates [9]:

$$\tau = \mu\dot{\gamma} + \tau_0 \quad (1)$$

Where τ is the shear stress [Pa], τ_0 is the yield stress [Pa], μ is the plastic viscosity [Pa·s] and $\dot{\gamma}$ is the shear rate [s⁻¹].

Since 1983 both new equipment [10-13] and useful interpretation approaches such as use of the rheographs [1] have been introduced. As a result the “concrete society” has finally started to understand benefits and importance of using the fundamental rheological parameters from this two point model instead of some values obtained by different empirical tests.

Even though portable equipment for determining Bingham parameters has been developed [12] and even a device that combines sample mixing and rheological measurements [13], concrete viscometers and rheometers are still considered luxury at the building sites, production plants and even at research institutions. In a lot of cases, in particular at the building sites, the slump cone invented more than a century ago [14] is much more popular due to its simplicity in handling and robustness. As a result, people have tried to evaluate the Bingham parameters from the results obtained by such simple methods. Like by the means of slump or slump-flow measurements. Such measurements can't be considered to be very accurate since the relationship to Bingham parameters is very complex and can vary also depending on the concrete composition [15-16]. However, in some cases these results can be more helpful than just plain empirical test data because they give quantitative values. Such information can be used for further analysis or calculations. In addition it is essential to have a relation between the viscometer results that is the new concrete research standard and the slump cone results that is the most widespread tool in the industry. In fact already in the original work by Tattersall and Banfill [9] they reported a relation between slump and yield stress of concrete obtained by different researchers in the middle of 1970's.

Today it is generally known that slump is influenced by both yield stress and plastic viscosity. However, for most cases the effect of plastic viscosity on slump is negligible [16]. Equations have been developed for calculating yield stress in terms of slump or slump-flow, based on analytical, numerical or experimental analyses [15-21, 25-29]. It must be noted here that efforts to relate the so-called stoppage tests (slump, slump-flow etc.) to the plastic viscosity of the tested samples have also been made. The measured values with these test methods give almost no indication of the plastic viscosity [16, 22]. The latter can to some extent be related to flow-time measurements of self-compacting concrete [23].

1.4. Objectives

In this paper the applicability of a slump-flow and yield stress relationship to SCC is investigated. The model [21] has not yet been verified for SCC and for experimental results obtained by coaxial cylinders viscometers (such as BML and Viscometer 5). In the original work presented by Roussel, Stefani and Leroy [21] it gave promising results for very flowable cement pastes.

The purpose of this project is to contribute to the further development of the elegant and simple concept proposed by the authors [21] and to give an insight into the possibilities and limitations of simple alternative yield value determination methods for SCC.

2. ATTEMPTS TO RELATE CONCRETE YIELD STRESS AND SLUMP OR SPREAD VALUES

Several efforts to relate fundamental rheological parameters of concrete to those measured with standard workability tests have been made. The research has shown that slump and slump-flow

or other so called stoppage test results generally have a reasonable correlation with the yield stress. The proposed solutions to the problem vary from simple curve fitting based on some limited experimental data to numerical simulations and analytical flow models [15-21, 25-29]. Some comparison can be found in the references [15, 24]. Though an overall criticism of the work introducing slump or spread and yield stress relation equations would be the uncertainties with rheological measurements – especially in the “early” papers that have been published before 2000. Some papers do not include any experimental validation at all.

According to Tattersall and Banfill [9] Moringa (1973 as cited in [9]) could be the first one that used experimental data to propose a linear equation based on simple curve fitting. The relationship showed that slump value can be negatively correlated to the measured yield value. Note that the plastic viscosity was excluded from the relation starting with this very first observation.

Further on other authors have tried the same. Among them Murata and Kikukawa [17] have used a coaxial cylinders rheometer to develop an empirical equation for yield stress τ_0 and slump s relationship. According to Murata and Kikukawa [17] Equation (2) is only valid for mixes with slump ranging from 125 to 260 mm (thus not applicable to most SCC cases):

$$\tau_0 = 714 - 473 \log(s) \quad (2)$$

In his Ph. D. thesis Hu (as cited in [18]) has used a finite element model of a slump test to develop an expression for yield stress in terms of slump value s and density of a concrete mix ρ , as shown in Equation (3):

$$\tau_0 = \frac{\rho}{270} (300 - s) \quad (3)$$

The finite element analysis has been performed for concrete with a slump value as high as 250 mm. According to Hu and co-workers [18] the recommended limitation of the expression is that it cannot be applied for concrete with plastic viscosity greater than 300 Pa·s. If the resistance to flow is higher they believe that viscosity sufficiently slows the flow and causes thixotropy, resulting in a reduction of the actual slump value. Equation (3) has been validated using results from the BTRHEOM rheometer and has shown a “satisfactory” agreement with measured values [18]. It must be noted here that already in 1989 Tanigawa and Mori [25] had used a viscoplastic finite element model introducing a frictional interface law at the base of the slump cone to develop a three-dimensional graph where slump, yield stress and plastic viscosity were related for concrete with slump in the range of 10 to 260 mm. However, they did not have any equipment to determine concrete rheological parameters experimentally, thus their results were not compared to experimental measurements.

Later Equation (3) has been further developed by Ferraris and de Larrard [19], de Larrard [20] and Wallevik [16]. They have used experimental results with more different concrete compositions and some other assumptions. Wallevik [16] proposed to normalize Equation (3) (to fit his experimental data) with respect to the volume fraction of matrix used in the concrete. Slump measurements seemed to be much more sensitive to the matrix volume differences than yield stress measurements in a coaxial cylinders viscometer. Wallevik also concluded that the trend line between slump and yield stress becomes more dependent on the matrix volume

fraction as the concrete becomes less workable. Thus it should be much less noticeable in the case of SCC.

Several analytical models (with some reasonable simplifications) have been developed to relate slump or slump-flow value to the corresponding yield stress. The models are derived from first principles with model variables expressed in dimensionless form. They are not material-dependent and provide a unique relationship between the yield stress and slump height or slump-flow diameter. One of the first models has been derived by Murata [26], followed by Christensen (1991 as cited in [27]) who corrected a simple integration error in the Murata's approach. They have proposed a relation between slump and yield stress that is based on assumption that slump cone can be divided in two parts. In the upper part the shear stress is lower than the yield of the material and no flow occurs. While in the lower part of the cone the shear stress from self-weight of the fresh concrete is higher than the yield stress and flow occurs. Then the flow criteria would be the concrete cone height that must reduce until shear stress in the flow zone is equal to the yield. Rajani and Morgenstern (1991 as cited in [27]) and Schowalter and Christensen [27] have further investigated this kind of conical test. They proposed another relation between final total height of the cone and the yield stress that did not depend on the mould geometry. Later verification [28-29] of their assumptions suggested that non-dependency on the mould geometry in fact means that the model would generally work only for very flowable concrete, i.e. with high slump or low yield stress. It also demonstrated that the relation is suitable when cylindrical mould geometry is used but in case of conical mould (such as ordinary concrete slump cone) a discrepancy between predicted and measured slump values was systematically obtained.

It must be noted here that all of the above mentioned analytical approaches involve a uni-dimensional expression of the yield criterion, i.e. the flow occurs or stops when the shear stress becomes higher or lower than the yield stress. By using this formulation other stress tensor components are not taken into account and thus the analysis of flow is greatly simplified [15]. A scalar yield criterion derived based on such formulation is then only valid for shear dominated flow. In fact it would only be true for ideal two-dimensional flow [15]. Roussel [15] has thus used a three-dimensional yield criterion to develop numerical simulations of free surface stoppage flow (such as concrete slump measurements). He has also validated the numerical values with experimental results from both BML and BTRHEOM viscometers. Results obtained by BTRHEOM viscometer showed a rather good relation to the numerically obtained values. With respect to the above mentioned and as reported in [30], results obtained by BML viscometer have also showed a rather good relation to the numerical values. However, due to some approximations when modelling, the flow numerical results obtained by Roussel [15] are not valid for mixes with a slump values higher than 250 mm. Thus this approach can't be used for SCC.

Yet a much simpler model using different assumptions has been at the same time introduced by Stefani, Leroy and Roussel [21]. They proposed an analytical approach to relate spread of a cementitious suspension measured by any geometry of a truncated slump cone to yield stress of the same material. Among others their model is especially designed for mixes with low yield. However, the model was originally developed for cement pastes and grouts and has not been validated for SCC. The model [21] is based on the fact that if the shear stress in the tested sample becomes smaller than the plastic yield value (the plasticity criterion is not fulfilled any more), the flow stops.

Geometry of a cylindrical slump-cone of interest is given in Figure 1. Stefani, Leroy and Roussel [21] describe the motion during slump-flow test within the frame of long-wave approximation: the characteristic length of the contact surface in the horizontal plane is much larger than the characteristic length of fluid depth. It must be emphasized here that this will not be true for tests performed on mixes with high yield value or according to them [21] for slumps strictly higher than 200 mm. Then by the use of long wave approximation, in cylindrical coordinates, in case of axial symmetry and when the inertia is neglected the equilibrium equations simplify to:

$$\frac{\partial p}{\partial r} = \frac{\partial \tau}{\partial z} \quad (4)$$

$$\frac{\partial p}{\partial z} = -\rho g \quad (5)$$

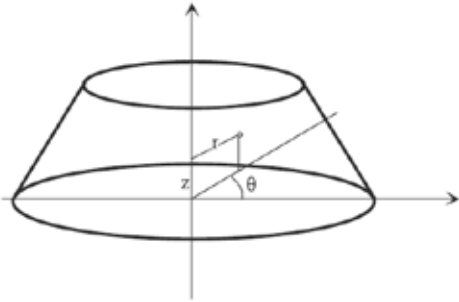


Figure 1 – Initial cone shape and cylindrical coordinates [21].

Distribution of the pressure p is assumed to be hydrostatic, as reported to usually be found for various types of free surface flow, even for yield stress fluids [21]:

$$p = \rho g(h(r) - z) \quad (6)$$

where

p = pressure distribution;

ρ = volumetric weight of the cement-based material (=concrete density);

g = gravitational acceleration;

r = initial radius of the cone shaped cement-based material;

h = initial height of the cone shaped cement-based material as the function of radius (spread);

z = pressure reference point; the pressure for $z=h(r)$ equals the atmospheric pressure which is taken as the reference point.

Then by using assumptions that surface tension effects are small compared to the yield consequences and about the shape of the material at stoppage Roussel, Stefani and Leroy [21] found:

$$\tau_0 = \frac{225\rho g V^2}{128\pi^2 R^5} \quad (7)$$

where

V = tested sample's volume;

R = radius of the measured flow (half the slump-flow value).

Experimental results on several cement pastes presented by Roussel, Stefani and Leroy [21] validated their assumption but also showed the necessity to take into account the surface tension effects for low yield stress materials. In order to take into account the surface tension effects they introduced another character in the Equation (7):

$$\tau_0 = \frac{225\rho g V^2}{128\pi^2 R^5} - \lambda \frac{R^2}{V} \quad (8)$$

The coefficient λ is a function of both the unknown tested fluid's surface tension and contact angle between the fluid and test surface. They assume that this coefficient is about the same for any cementitious material for a given test surface. The coefficient would depend on the chosen test surface and has to be identified for a given apparatus. In their study with cement paste testing Roussel, Stefan and Leroy [21] used a min-cone ($r=35$ mm; $R=50$ mm and $h=50$ mm) on smooth plastic test surface. Then by fitting the obtained spread to the predicted, a constant $\lambda=0.005$ was found independent of the mix flowability or composition. Then an excellent consistence with experimental data was achieved.

Based on the initially mentioned long wave approximation that was used when developing the model, sample stoppage shape limitation is $h \ll 2R$. As suggested by Roussel, Stefani and Leroy [21] this will only be valid in the range where the sample height is close to the size of the coarse aggregate, i.e. for SCC. They encourage that the proposed relation (Equation (8)) is further tested as simple and quick alternative interpretation of the slump-flow of a very flowable concrete. The purpose of this work is then to investigate the applicability of the model [21] to SCC.

2.1. Limitations regarding different viscometers

As stated by Wallevik [31] the art of science is also to know the limitations of tools you are applying. With respect to the results discussed here it would imply viscometer results since slump-flow measurements included in this study were all performed on plastic (slump > 70 mm) and stable concrete mixes by the same operator. All of the measurements have been performed according to the relevant CEN standard, i.e. EN 12350-8:2010 [32]. Hence, the slump-flow values can be considered to be reliable and only some regular repeatability issues should be remembered when analysing the results.

Two things should be considered that can be attributed to all concrete rheological investigations with the available equipment. These and some others that will not be mentioned include errors that make the measured yield stress values τ_0 dependant on the measurement technique. First an experimental error called particle migration can occur in any type or brand of viscometer [16, 33]. Particle migration is a shear rate introduced migration, and due to this phenomenon particles are moved away from the zone with the highest shear rate. A couple of reasons are proposed to explain particle migration [33] one of them being dilatancy or sample volume increase due to shearing movement. Since SCC generally has more matrix or cement paste than

CVC the latter is more prone to errors due to particle migration. Detailed explanation of the particle migration phenomenon can be found in the Ph.D. thesis of J.E. Wallevik [33].

Another important limitation is the viscometer type used. Since experiments have proven that the two most widely used viscometer types – ConTec’s viscometers (BML and Viscometer 5) and BTRHEOM viscometer generally will give different absolute values of yield stress τ_0 , even though the trend of the yield change is very similar when different mixes are tested [10-11, 33]. Systematic comparison of those devices, including also the Mk-system by Tattersall, showed that BTRHEOM measures a higher yield stress than either of the ConTec’s viscometers or by the Mk-system. A good agreement was shown to exist between the Mk-system and the ConTec’s viscometers while BTRHEOM measured roughly two times higher values [10-11, 33]. It has also been discussed that it is hard to conclude which one of them is giving the correct values and perhaps they could both be wrong or at least that none of them is correct on the entire range of yield stresses tested [15]. However, discussion of this kind is out of the scope of this paper. One should just keep in mind this limitation when using results from different viscometers and trying to relate them to slump or slump-flow values.

It must also be noted that in general the nature of the two test methods that are frequently tried to be related – viscometry and stoppage tests is quite different. Rotational viscometers like BML and BTRHEOM perform a dynamic test that is different from the slump test which starts with an impact and stops due to friction inside the material and against the base plate. This could be another much less investigated source of error in the attempts to relate concrete yield stress and slump or spread values.

3. MATERIALS AND METHODS

3.1. Concrete composition and mixing

Twenty different very flowable concrete and SCC mixes were studied in order to evaluate the possibilities of applying the given free flow model [21]. Mixes have been prepared during a previous work of the author [34] performed within COIN – Concrete Innovation Centre (www.coinweb.no). Thus exact concrete composition and test results can be found in the relevant reference and only the most important details will be given here.

Proportioning of the concrete mixes has been done following the Particle-Matrix model [8] with strict control of particle size distribution and volume fractions of particles and matrix. The initial goal of the study was to investigate how different types of mineral fillers (mainly crushed) affect on rheology of fresh highly flowable and self-compacting concrete. Thus three basic types of mix design have been prepared where the mineral filler type was kept as the only variable within those types (Table 1). All mixes were prepared using two fractions (0/8 and 8/16 mm) of natural aggregates. Total filler amount is given as volume fraction of cement. It includes also 7% of natural fines from “low-filler” 0/8 mm sand used for the batches. Polycarboxylate based superplasticizer (SP) was used for all of the mixes. The amount used is shown in Table 1 marked as % SP meaning percentage of the admixture (with solids content 30%) relative to cement weight. Norcem AS Standard Fly-ash cement (CEM II/ A-V 42.5 R) was used for all of the mixes. The parameter w/V_{powder} denotes water to powder (all particles smaller than 125 microns including cement) ratio on the volume basis that was used as a mix design parameter to ensure that mineral filler type was the only variable.

Table 1 – Mix compositions of the tested concrete batches

w/c	Matrix volume V_m [l/m ³]	Cement [kg/m ³]	% SP	w/ V_{powder}	% Filler
0.50	360	389	1.1	1.18	20
0.60	360	324	1.1	1.18	33
0.77	400	314	0.6	1.51	33

A Collomix ColloMatic® XM 2 - 650 forced action paddle-pan type mixer was used to prepare the SCC mixes utilizing the standard 6 minute mixing procedure according to EN 480-1:2011 [35]. On the average 8 minutes were used for mixing and transfer to the viscometer. Slump-flow measurements were performed parallel to rheological measurements.

3.2. Viscometer

All concrete rheological measurements have been performed with a Viscometer 5 by ConTec. The ConTec's Viscometer 5 has been designed as a coaxial cylinders viscometer. However, recently a parallel plate measuring system has also been reported to be available [36]. To measure the concrete consistency for the given mixes the coaxial cylinders system was chosen. It consists of an outer cylinder (of radius $R_o=0.145$ m) that rotates at predetermined frequencies f_o [rps], while the inner cylinder (of radius $R_i=0.100$ m and height $h=0.199$ m) is stationary and measures torque T [Nm]. Viscometer 5 has shown good relation to the results obtained by the use of the older and so far more popular coaxial cylinders equipment from ConTec (BML type viscometers) [37].

4. RESULTS AND DISCUSSION

Comparison of calculated and measured relationship between slump-flow SF and yield stress τ_0 of the concrete mixes is shown in Figures 2 and 3. Calculated yield values shown in Figure 2 are obtained by Equation (7), i.e. by neglecting the surface tension effects. In Figure 2 all results are included, i.e. also with $SF < 550$ mm. From data presented it can be seen that a good relation between calculated and measured yield values can be retained only for slump-flow values not lower than approximately 550 mm. This is, however, the lowest SCC workability reported to be used in practical applications, in particular in combination with very low viscosity to produce the so called “high-yield SCC” [1].

No dependence on the mix compositions as in the work by Wallevik [16] can be observed. This is neither expected as in [16], such dependency only start to emerge with yield stress greater than about 200 Pa. In the same way there is also no clear relationship between the measured plastic viscosity and yield stress τ_0 (Figure 4). In general it seems that for a given w/c ratio a higher viscosity somewhat tends to correspond to a higher yield stress and this trend seems to be more pronounced as the w/c ratio decreases.

Figure 2 also reveals some possible problems with the viscometers as discussed in Section 2.1. As the mixes tend to get stiffer, some unexpected deviations from the general trend seem to appear. This can be perceived by looking at the three data points on the very left of the plot in Figure 2, which represent the three less flowable mixes. The slump flow of those mixes is almost constant, i.e. 380, 390 and 395 mm while the measured yield stresses are 133, 133 and 46 Pa accordingly, i.e. varying by a factor of approximately 3. There are in general two possible

explanations for this. First, the plastic viscosities of the mixes are 72, 59 and 48 Pa·s accordingly which means that a higher plastic viscosity also gives a higher yield stress for a given slump-flow. The second explanation would then be related to the effects that are observed due to shortcomings of the yield stress measuring method, i.e. Viscometer 5 (please see Section 2.1. for further discussion on this). Taking into account also the results from Figure 4, it is reasonable to say that most likely the deviation of the given three data points from the general trend is a combination of both the mentioned factors, i.e. influence of the plastic viscosity and shortcomings of the Viscometer 5. To make things right, it must be mentioned here, that no direct critics should be addressed specifically to Viscometer 5. There is a strong basis [10-11, 33] to think that the same problems would arise with other types of the widely available viscometers. Then a general conclusion would be that development of the models where workability expressed with slump or slump-flow values is related to the corresponding rheological parameters (such as yield stress and plastic viscosity) are in fact ahead of the evolution of the available measuring equipment. This means that perhaps more effort should be put into development of the viscometers, since otherwise there are no actual possibilities to feasibly verify any of the proposed models.

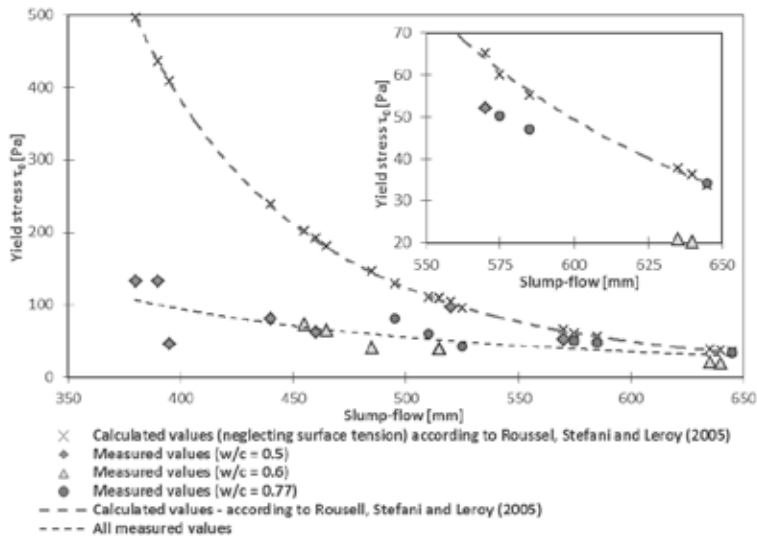


Figure 2 – Plot of all measured and calculated (neglecting surface tension effect) yield stress τ_0 values as a function of slump-flow (main illustration) and the same values for the SCC workability region (small illustration)

In the small integrated illustration of Figure 2 the region of interest (with $SF > 550$ mm or SCC workability region) is shown in a bigger scale. It can then be observed that the measured values fall below the predicted ones. This is the same relation that Roussel, Stefani and Leroy [21] found when neglecting the surface tension effects. In Figure 3 the calculation of the measured values (only for $SF > 550$ mm) is then done by Equation (8), thus by taking into account the surface tension. Then by fitting the measured yield stress data to the predicted values the constant λ was found to be 0.5. No clear λ dependence of the mix flowability or composition can be observed. Since the plot in Figure 3 is now in a bigger scale than in Figure 2 one might wonder why the calculated values (the crosses) do not perfectly coincide with the model expression. To make it clear, it must be explained that the calculated values in Figure 2 and Figure 3 would

not fit perfectly to the model trendline just because the model trendline has been constructed based on some average concrete density while the density is actually a bit varying for each single concrete mix. This then means that each of the concrete mixes would in fact have a separate model trendline that would deviate from the average one to a small extent due to the density variation.

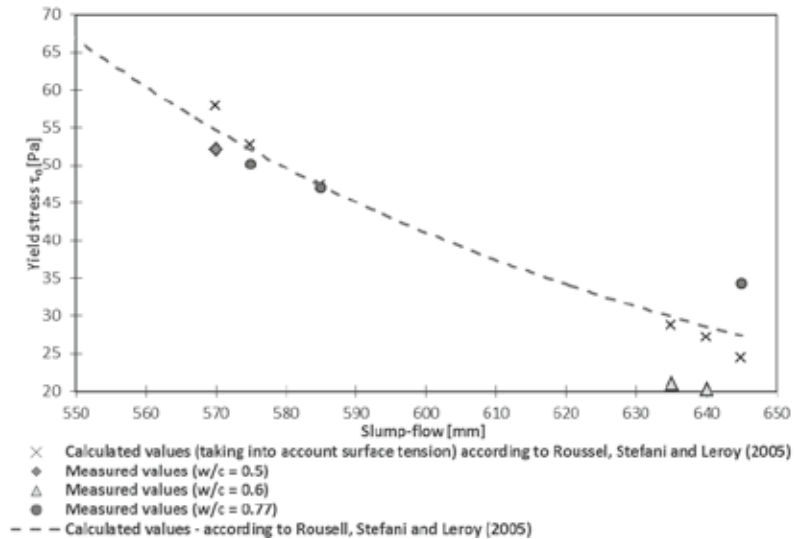


Figure 3 – Plot of measured and calculated (taking into account surface tension effect) yield stress τ_0 values as a function of slump-flow for SCC workability region

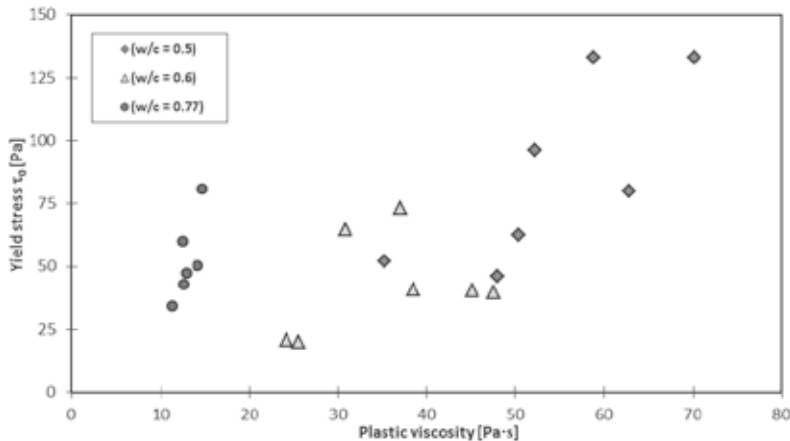


Figure 4 – Plot of measured yield stress τ_0 values as a function of the measured plastic viscosity

Comparison of the calculated and measured yield stress values presented in Figure 3 is only visual based. To quantify it further, relative yield stress values (results from Equation (8) with $\lambda=0.5$ / measured values by Viscometer 5) are plotted against the measured slump-flow values in Figure 5. As it can be seen from the figure, the relative yield stress values for the SCC range (i.e. SF > 550 mm) fit close around the unity; with a maximum deviation value of 0.71 and the

average of 1.10. This means that the calculated values are on average by only 10% higher than the measured ones. However, it must also be taken into account that there are in fact only 6 data points that apply for the average deviation calculation.

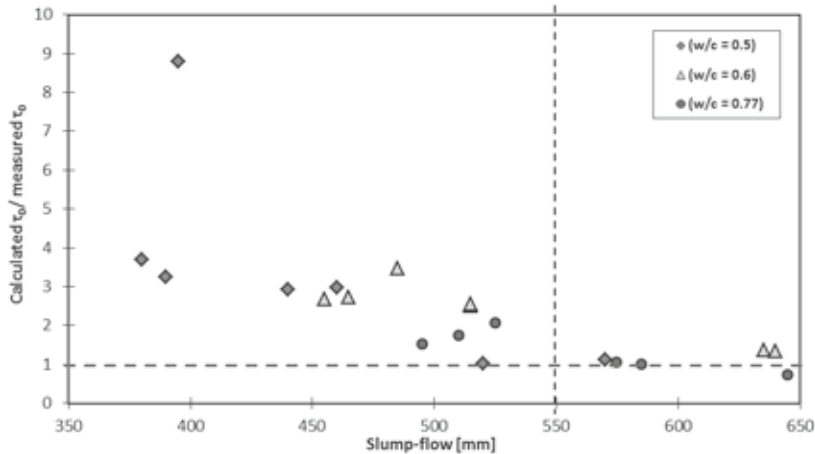


Figure 5 – Plot of relative yield stress values (results from Equation (8) with $\lambda=0.5$ / measured values by Viscometer 5) as a function of measured slump-flow

5. CONCLUSIONS

Literature review has revealed that even though different analytical models of stoppage tests (slump and slump-flow) and yield stress relationship have been developed from various approximations, no single universal relation exists. It would be recommended to use different equations at least for CVC and SCC or even better calibrate a relationship for each type of concrete if more precise results are necessary.

Based on mixes covering both CVC and SCC tested with slump-flow and rotational viscometry it has been demonstrated that the model by Roussel, Stefani and Leroy [21] seems to be applicable for fresh concrete with a slump-flow higher than 550 mm, i.e. the range that is practically used for SCC. However, further investigations are recommended to get a complete understanding regarding the limitations of the given model.

When concluding one should remember the limitations discussed in Section 2.1 where difference between results obtained by different viscometers have been described. Some possible shortcomings of the used viscometer are thought to be seen also for the results discussed in this work. Then perhaps a general conclusion would also be that development of the models where workability expressed with slump or slump-flow values is related to the corresponding rheological parameters (such as yield stress and plastic viscosity) are in fact ahead of the evolution of the actual measuring equipment. This means that perhaps more effort should be put into development of the viscometers, since otherwise there are no actual possibilities to feasibly verify any of the proposed models.

ACKNOWLEDGEMENTS

The results presented here are based on work performed in COIN – Concrete Innovation Centre (www.coinweb.no) – which is a Centre for Research based Innovation, initiated by the Research Council of Norway (RCN) in 2006. The author also would like to personally acknowledge Øystein Mortensvik (Rescon Mapei AS) for help with running the viscometer and prof. Stefan Jacobsen (NTNU) for reviewing the paper.

REFERENCES

1. Wallevik, O.H. and Wallevik, J.E., 2011. Rheology as a tool in concrete science: The use of rheographs and workability boxes. *Cement and Concrete Research*, V. 41, pp. 1279-1288.
2. Wallevik, O.H., 2011. A green alternative to self-compacting concrete. *The Singapore Engineer*, February issue, pp. 13-18.
3. Peterson, M., 2008. *High-performance and self-compacting concrete in house building. Field tests and theoretical studies of possibilities and difficulties*. Ph. D. Lund University.
4. Simonsson, M., 2011. *Buildability of Concrete Structure. Processes, Methods and Materials*. Ph. D. Luleå University of Technology.
5. Emborg, S. and Simonsson, M., 2010. Increasing the market share of SCC. *Concrete Plant International*, 3, pp. 218-222.
6. Neville, A.M., 1995. *Properties of Concrete. 4th and final edition*. Harlow: Longman.
7. Mehta, P., 1999. Advancements in Concrete Technology. *Concrete International*, June issue, pp. 69-76.
8. Mørtzell E., 1996. *Modelling the effect of concrete part materials on concrete consistency*. Ph. D. Norwegian University of Science and Technology (In Norwegian).
9. Tattersall, G.H., Banfill, P.F.G, 1983. *The Rheology of Fresh Concrete*. London: Pitman Books.
10. Ferraris, C.F. and Bowler, L., eds., 2001. *Comparison of concrete rheometers: international tests at LCPC (Nantes, France) in October 2000*. NIST (National Institute of Standards and Technology) Report 6819. Washington: NIST.
11. Ferraris, C.F. and Bowler, L., eds., 2004. *Comparison of concrete rheometers: international tests at NB (Cleveland OH, USA) in May 2003*. NIST (National Institute of Standards and Technology) Report 7154. Washington: NIST.
12. Wallevik, O.H. and Hjartarson, B., 2006. Rheometer-4SCC, a Portable Rheometer for Self Compacting Concrete. In: *Proceedings of NordDesign Conference 2006*. Reykjavik, Iceland 16th-18th August.
13. Kubens, S., et. al., 2008. Some effects of silica fume on variations in rheology of mortar due to production date of cement. In: *Annual Transactions of Nordic Rheology Society, Vol. 16, The 17th Nordic Rheology Conference*. Copenhagen, Denmark 27th-29th August.
14. Bartos, P.J.M., Sonebi, M. and Tamimi, A.K., eds., 2002. *Workability and Rheology of Fresh Concrete: Compendium of Tests; Report of RILEM Technical Committee TC 145-WSM, Workability of Special Concrete Mixes*. Paris: RILEM Publications SARL.
15. Roussel, N., 2006. Correlation between yield stress and slump: Comparison between numerical simulations and concrete rheometers results. *Materials and Structures*, 39, pp. 501-509.
16. Wallevik, J.E., 2006. Relationship between the Bingham parameters and slump. *Cement and Concrete Research*. V. 41, pp. 1214-1221.

17. Murata, J. and Kikukawa, H., 1992. Viscosity Equation for Fresh Concrete. *ACI Materials Journal*, 89(3), pp. 230-237.
18. Hu, C. et. al., 1996. Validation of BTRHEOM, the new rheometer for soft-to-fluid concrete. *Materials and Structures*, 29(194), pp. 620-631.
19. Ferraris, C.F. and de Larrard, F., 1998. *Testing and Modeling of Fresh Concrete Rheology*. NIST (National Institute of Standards and Technology) Report 6094. Washington: NIST.
20. De Larrard, F., 1999. *Concrete mixture proportioning: a scientific approach*. London: E & FN Spon.
21. Roussel N., Stefani C. and Leroy R., 2005. From mini-cone test to Abrams cone test: measurement of cement-based materials yield stress using slump tests. *Cement and Concrete Research*, 35, pp. 817-822.
22. Geiker, M.R. et.al., 2002. On the Effect of Coarse Aggregate Shape on the Rheological Properties of Self-Compacting Concrete. *Cement, Concrete and Aggregates*, V. 24, pp. 3-6.
23. Zerbino, R. et. al., 2009. Workability tests and rheological parameters in self-compacting concrete. *Materials and Structures*, 42, pp. 947-960.
24. Koehler, E.P. and Fowler, D.W., 2003. *Summary of Concrete Workability Test Methods*. Research Report – 105-1. Austin: ICAR.
25. Tanigawa, Y. and Mori H., 1989. Analytical study on deformation of fresh concrete. *Journal of Engineering Mechanics*, 115 (3), pp. 493–508.
26. Murata, J., 1984. Flow and Deformation of Fresh Concrete. *Materials and Structures*, 98, pp. 117–129.
27. Schowalter, W.R. and Christensen, G., 1998. Towards a rationalization of the slump test for fresh concrete: Comparison of calculations and experiments. *Journal of Rheology*, 42 (4), pp. 865–870.
28. Clayton, S., Grice, T.G. and Boger, D.V., 2003. Analysis of the slump test for on-site yield stress measurement of mineral suspensions. *International Journal of Mineral Processing*, 70, pp. 3-21.
29. Saak, A.W, Jennings, H.M. and Shah, S.P., 2004. A generalized approach for the determination of yield stress by slump and slump-flow. *Cement and Concrete Research*, 34, pp. 363–371.
30. Rousell, N., et.al., 2007. Computational modelling of concrete flow: General overview. *Cement and Concrete Research*, 37, pp. 1298-1307.
31. Wallevik, O.H., 2011. Rheology and measurement techniques, *T-845-RHEO Rheology of Cementitious Materials*. Reykjavik University, unpublished.
32. European Committee for Standardization, 2003. EN 12350-8:2010 *Testing fresh concrete - Part 8: Self-compacting concrete - Slump-flow test*. Brussels: CEN.
33. Wallevik J., 2003. *Rheology of Particle Suspensions. Fresh Concrete, Mortar and Cement Paste with Various Types of Lignosulfonates*. Ph. D. Norwegian University of Science and Technology.
34. Cepuritis, R., et.al., 2012. *Rheology of Matrix and SCC with Different Mineral Fillers and Admixtures*. COINProject report x – 2012, unpublished.
35. European Committee for Standardization, 2011. EN 480-1:2011 *Admixtures for concrete, mortar and grout - Test methods - Part 1: Reference concrete and reference mortar for testing*. Brussels: CEN.
36. Wallevik, J.E., 2009. *Development of parallel plate-based measuring system for the ConTec viscometer*. In: Proceedings of the 3rd International RILEM Symposium on Rheology of Cement Suspensions such as Fresh Concrete. Reykjavik, Iceland 19th–21st August.

37. Wallevik, O.H., 2003. Rheology – a scientific approach to develop self-compacting concrete. In: *Proceeding 3rd International Symposium of Self-Compacting Concrete*. Reykjavik, Iceland 17th-20th August.

Simplified Methods for Crack Risk Analyses of Early Age Concrete

Part 1: Development of Equivalent Restraint Method



Majid Al-Gburi
M. Sc. Ph.D. Student
Lulea University of Technology
Dept. of Structural Engineering
Email: majid.al-gburi@ltu.se



Dr. Jan –Erik Jonasson
Professor
Lulea University of Technology
Dept. of Structural Engineering
Email: jej@ltu.se



Dr. Martin Nilsson
Lulea University of Technology
Dept. of Structural Engineering
Email: martin.c.nilsson@ltu.se



Dr. Hans Hedlund
Adjunct professor
Skanska Sverige AB
and Lulea University of Technology
Dept. of Structural Engineering
Email: hans.hedlund@skanska.se



Anders Hösthagen
M. Sc. Ph.D. Student
Projektengagemang AB
and Lulea University of Technology
Dept. of Structural Engineering
Email: anders.hosthagen@projektengagemang.se

ABSTRACT

The present study deals with both the compensation plane method, CPM, and local restraint method, LRM, as alternative methods studying crack risks for early age concrete. It is shown that CPM can be used both for cooling and heating, but basic LRM cannot be applied to heating. This paper presents an improved equivalent restraint method, ERM, which easily can be applied both for usage of heating and cooling for general structures. Restraint curves are given for two different infrastructures, one founded on frictional materials and another on rock. Such curves might be directly applied in design using LRM and ERM.

Key words: Local restraint methods, compensation plane method, equivalent restraint method, crack risk, early age concrete.

1. BACKGROUND

Over the past few decades, a continuous progress in the research and understanding of the effect of the early mechanical and visco-elastic behaviour of concrete has been presented, see e.g. [1], [2], [3], [4] and [5]. The main phenomenon causing early age cracking is volume change due to the variable moisture and temperature state in the concrete. With the use of high-performance concrete (low water cement ratio, high cement content) the volume changes increase because of the elevated heat of hydration and high autogenous shrinkage. Early-age thermal cracking is a result of the heat produced during hydration of the binder. Cracking originates either from different expansions (due to temperature gradients inside the young concrete during heating, which may result in surface cracking) or by restraint from the adjacent structure during the contraction phase, (the result of which may cause through cracking). For ordinary concrete structures, like tunnels, bridges, etc., surface cracking occurs within a few days, and through cracking occurs within a few weeks. Pre-calculation of stresses in young concrete is performed with the aim of analyzing the risk of these cracks occurring. If the crack risk is too high, actions are needed to prevent the cracking. Common actions on site are cooling of the young concrete and/or heating of the adjacent structure. Restraint from the adjoining structures is the main cause of through cracking. Unfortunately, for complex structures, it is an uncertain factor because it is hard to estimate [6].

The most general approach of modelling early age structures is 3D FEM analyses. This entails realistic modelling of young concrete and the bond between different parts of the structure. The method is very complex and therefore, in practice, it is replaced by different simplified methods, such as: the three-step engineering method, the compensation plane method, one-point calculation. These methods are described amongst others in [6], [7] and [8].

The focus of this study is devoted to establishing and applying restraint curves. To simplify crack risk calculations based on restraint curves, an improved method, denoted equivalent restraint method, is presented in the paper.

2. AIMS AND PURPOSE

The aims and purpose of this paper are to:

- Clarify the difference between the CPM (compensated plane method) and the LRM (local restraint method).
- Estimate and compare stresses using CPM and LRM for cases where the CPM conditions are fulfilled.
- Establish an engineering approach to crack risk analyses using local restraint curves for general structures and to be able to incorporate actions taken on site (heating/cooling).
- Analyze restraint situations for some typical infrastructures.

3. THE COMPENSATION PLANE METHOD

3.1 Classical Japanese method

The compensation plane method (CPM) was developed in 1985 as a calculation program that can be widely applied for thermal stress analyses of massive concrete structures, [9] and [10]. This method is based on the assumption of linear strain distribution, which is equivalent to the statement that plane sections remain plane after deformations [11]. The cross-section is divided into discrete elements with individual temperature and level of maturity. The initial stress in the

cross section is shown in the left part of figure 1. The sum of internally hindered stress, that is derived from the difference between the compensation plane and temperature distribution curve, is shown in the right part of figure 1. The externally restrained stresses are equivalent to the stresses caused by the forces, i.e. axial force N_R , and bending moment M_R , required to return the plane after deformation to the original restrained position, [9] and [10]. N_R and M_R are given by the following equations using external restraining coefficients R_N and R_M , respectively.

$$N_R = R_N EA \bar{\epsilon} \quad (1)$$

$$M_R = R_M EI \bar{\varphi} \quad (2)$$

where E , A and I are cross-section parameters; E is the Young's modulus; I is the moment of inertia; A is the cross-section area; $\bar{\epsilon}$ is axial strain increment; and $\bar{\varphi}$ is the gradient as curvature increment.

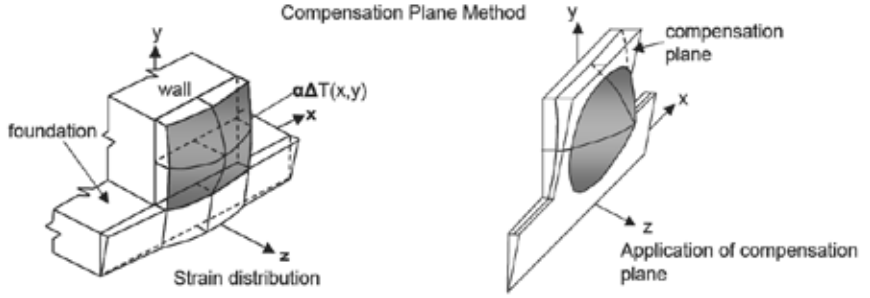


Figure 1 - Illustration of compensation plane method [10].

Different levels of maturity and stiffness can be taken care of in various parts of the cross-section, where the stress distribution is displayed and the compensation plane is considered [6]. The external restrained coefficients were derived from numerical calculation by the three-dimensional finite-element method. Finally, the initial stress $\sigma(x, y)$ at a position with coordinates (x, y) is given by the following equation, [9] and [10].

$$\sigma(x, y) = E_i \{ \epsilon_0(x, y) - \bar{\epsilon} - \bar{\varphi}(y - y_g) \} + R_N E_i \bar{\epsilon} + R_M E_i \bar{\varphi}(y - y_g) \quad (3)$$

where E_i is the Young's modulus at position (x, y) ; ϵ_0 is the initial strain; y_g is the centre of gravity for the whole cross-section.

The advantage of CPM compared to full 3D early age analysis is clear, as the number of the unknowns is strongly reduced, [6] and [10]. If CPM is formulated in the simplest way, the number of unknowns is only 3: one translation and two curvatures. Besides, both computational time and time spent on the modelling and surveying of the results are largely decreased using CPM.

3.2 Non-plane section analyses

The classical compensation plane method, assumes that plane sections remain plane after deformation, which is only theoretically valid for high length to height ratios (L/H), approximately 5 or more (this is comparable to classical beam theory). However, in many real cases for thermal cracking, the length to height ratios is lower. In these cases, the assumption of

plane sections is no longer valid. One way of taking this into account is to define restraint factors at different heights for various L/H ratios, see figure 2 from [12]. The restraint factors in figure 2 can be used directly in cases where we have a small volume of newly cast concrete on very large or very stiff foundations. For a finite foundation and pure translation, a multiplier, δ_f , can be applied together with restraint factors [1] as:

$$\delta_f = 1/(1 + A_C E_C / A_F E_F) \quad (4)$$

where A_C and A_F are cross section areas of new concrete and old foundation respectively; E_C and E_F are modulus of elasticity for new concrete and old foundation.

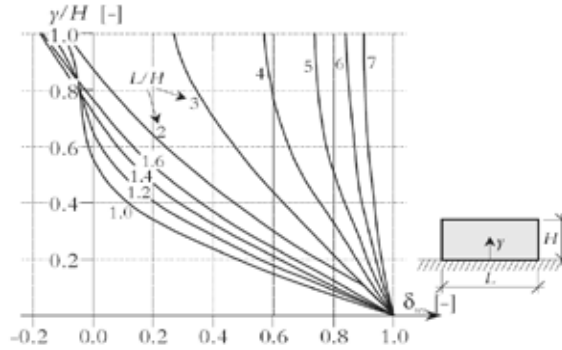


Figure 2 – Restraint factors for walls on stiff foundation [12].

Furthermore, for the case of massive concrete on rock, the effective restraining rock area A_F can be assumed to be $2.5 A_C$ [1].

Implementation of the restraint factors to the compensated plane method has been performed in the following steps [2]:

- a. Reduction of the initial strains according to the restraint factors for the L/H ratio in question for fixed strains ($R_N = R_M = 1$).
- b. Adding the axial deformation, if $R_N < 1$.
- c. Adding the rotational deformation, if $R_M < 1$.

One way of performing stress calculations in young concrete is to assume full adhesion in the joint between the newly cast concrete and the adjoining structure. Based on this assumption, an elastic calculation, where the wall is homogeneously contracting, will show results of maximum and minimum principal stresses like those shown in figure 3 from [13]. From the figure, it is seen that the principal stresses are, not unexpectedly, highest in the corner portion at the end of the construction joint (point A). However, generally speaking, cracking actually occurs as almost vertical cracks in the central part of the wall, see figure 3b. The overall conclusion from this discrepancy between theory and practice is that full adhesion cannot be present and slip failure occurs, initiating from the end of the joint (point A), see figure 4.

Assuming full adhesion is correspondingly too conservative, in particular for moderate structural lengths ($L < 6\text{m}$) [13]. Usually macro cracks are not observed at the joint, which can be interpreted as an occurrence of micro cracks at the end corner of the wall. This may be denoted joint "slip failure" or "micro cracking" at the end of the wall. Based on the conclusions

in [13], a slip factor has been introduced into the compensation plane method, [14], [15] and [16], see figure 5. The use of restraint factors together with slip factors for the compensation plane method, for a constant initial strain in the young concrete, is illustrated in figure 6 [14].

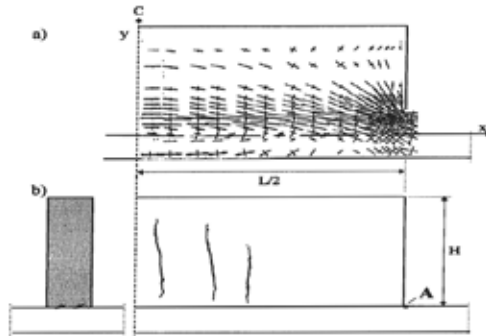


Figure 3 - Calculated maximum and minimum principle stresses for structure wall-on-slab using 2D elastic FEM [13].

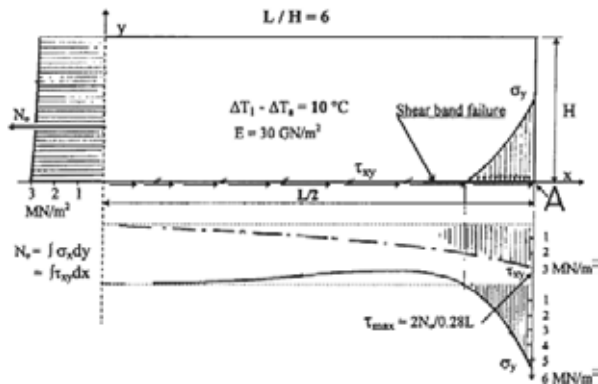
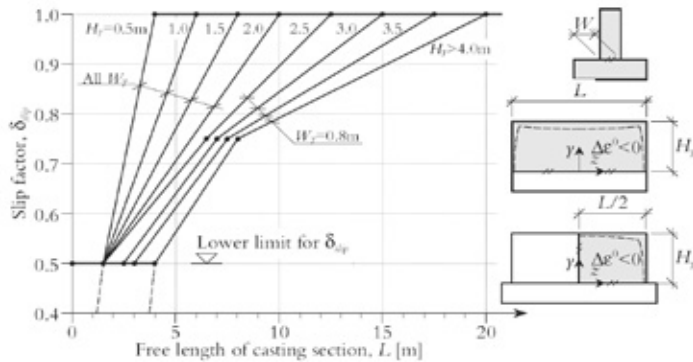
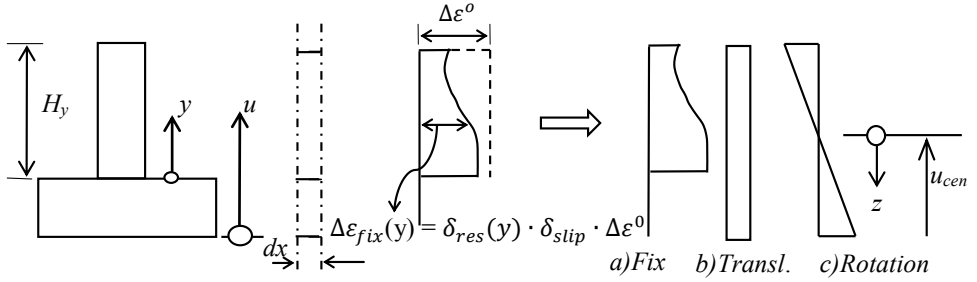


Figure 4 - Illustration of progressive joint failure starting at the end of the joint [13].



Figures 5 - Slip factor as function of free length (L), height (H) and width (W) of the wall, [14], [15] and [16].



Figures 6 – Illustration of compensated plane method for non-plane section analyses [14].

The introduction of restraint factors in step “a)Fix” reducing the initial strain, see the term “ $\Delta\epsilon_{fix}(y) = \delta_{res}(y) \cdot \delta_{slip} \cdot \Delta\epsilon^0$ ” in figure 6, shows a simplified method to take into account a non-plane section (factor $\delta_{res}(y)$, see figure 2) and, if any, effects of local micro cracking (δ_{slip} , see figure 5). An alternative approach may be to introduce the local restraint method together with, if any, the slip factor (δ_{slip}), see further chapter 4.

4. THE LOCAL RESTRAINT METHOD

The method presented here is a point wise calculation denoted LRM (local restraint method). The LRM is primarily used for the evaluation of the restraint effect for a homogenous contraction in the newly cast concrete. If the new concrete is free to move, there will be no stresses in the concrete. But, if the young concrete is cast on an adjoining existing structure, stresses will arise in the concrete due to the restraining actions from the adjacent structure. The uniaxial restraint effect, R_i , is defined as:

$$R_i = \frac{\sigma_{ui}}{(-\Delta\epsilon^0 E_C)} \quad (5)$$

where σ_{ui} = resulting stress from the elastic calculation, where i = a chosen direction in the concrete body; u = uniaxial coordinate in i direction; $\Delta\epsilon^0$ = the homogenous contraction in the concrete; and E_C = Young’s modulus in the early age concrete.

If the temperature caused by hydration of the new concrete is uniform, LRM is theoretically correct. In real cases, the temperature in young concrete is more or less non-uniform. Fortunately, in most civil engineering structures, the temperature is symmetric in the direction of the smallest dimension as well as constant in the perpendicular direction. In such cases, the average temperature through the thickness is representing a homogenous contraction with respect to the risk of through cracking. For cases where the temperature distribution in the young concrete neither is symmetric in direction of the smallest dimension nor constant in the perpendicular direction, the assumption of homogenous contraction is no longer valid.

The basic LRM formulation is a good engineering model provided no heating/cooling measures are taken on site. LRM might also be applicable for calculation of stresses when cooling is used, provided the changes in restraint caused from cooling can be neglected. Unfortunately the basic LRM is not applicable in cases where heating is used because the structural balance between the concrete and the adjoining structure caused from heating give rise to a more complicated strain situation.

In this study, restraint curves are created by 3D elastic calculations using Eq. 5. For the cases presented here, the direction i is parallel with the direction of the joint, which is in agreement with the findings in Bernander [13], see figures 3 and 4. This simplification is the typical situation for many civil engineering structures like bridges, tunnels, harbours, etc. In more complicated cases the direction of maximum principal stress might be relevant, and the actual situation has to be evaluated by the user.

5. CRACK RISK ESTIMATIONS AT EARLY AGES

5.1 General background

The estimation of the risk of cracking of early age concrete structures can be based on five steps, [1], [8], [9], [13], [17], [18], [19], [20], [21] and [22]:

The first step: When no measures are taken on site, certain principle factors can be chosen to avoid or reduce the risk of thermal cracking at early ages. The most important principal factors are the choice of the structure with respect to dimensions and casting sequences as well as selection of mix design.

The second step: Estimation of thermal temperature development during the hydration phase. This can be done either by calculations or from measurements in real structures. From the temperature development, the strength growth is obtained. The temperature calculation also includes factors such as insulation, cooling and/or heating or other measures possible to perform on site.

The third step: Estimation of the structural interaction between the early age concrete and its surroundings. This can typically be done in two different ways: either starting with an estimation of the boundary conditions for a structure including early age concrete and adjoining structures. Alternatively this can be achieved by an estimation of restraint factors, such as LRM in chapter 4, for direct calculation of different positions in the early age concrete.

The fourth step: Structural calculations resulting in stresses and strains in the young concrete. These are usually presented as stress/strength or strain/ultimate-strain ratios as a function of time.

The final step: Comprises of crack risk design using partial coefficients - or crack safety factors – as design conditions in different codes and standards.

The present study shows the application of LRM to estimate the crack risk in concrete at early age, primarily aimed for the situation without measures taken on site. For cases using cooling pipes or heating cables, an additional method denoted ERM (equivalent restraint method) is evaluated in the paper.

5.2 Application of local restraint method

Application of the local restraint method can be performed in two different ways, either by using an equivalent material block simulating the actual restraint factor in any position in the young concrete, or by direct use of the restraint factor for the position in question within the new concrete. The former procedure may be used in most computer programs for fresh concrete, see for instance [15], [17], [23] and [24] and in the present study the latter procedure is applied with the ConTeSt program [15].

In this paper two cases for typical wall-on-slab structures are studied. Comparison are made between calculated strain ratios using compensation plane method (CPM) and local restraint method (LRM), see examples 1 and 2. The restraint curves in this study are calculated using a similar method to that presented in [16] using uniform contraction in the young concrete, and the Young's modulus is 7 percent lower than in the adjoining concrete [25].

Example 1

Three wall-on-slab structures with different casting situations are considered with the dimensions according to [26]. The cross-section of the wall was constant, with the width of the wall 0.4m, and the height of the wall 2.25m. Different restraint conditions for the wall are applied in the three situations, all with free translation and free bending of the total structures, as follows:

- Wall 1 cast on slab 1, casting length (L_{cast}) = 6m.
- Wall 2 cast on slab 2, the wall cast against existing slab 2 and existing wall 1, L_{cast} = 6m.
- Wall 3 cast on slab 3, L_{cast} = 12m.

The free casting length, L_{free} , is defined as the length of a monolithic structure with two free ends. This means that $L_{free} = L_{cast}$ for cases a and c. For the case b, we have to imagine a free monolithic length that is twice the real casting length, i.e. $L_{free} = 2 \cdot L_{cast} = 12m$. The denotation L has the meaning L_{free} in the subsequent figures and text. The restraint is calculated using Eq. 5, and the resulting distributions in the walls for cases a-c are shown in figure 7, where y is the vertical coordinate, and $y = 2.5m$ at the joint between the slab and the wall. The figure shows that the distribution of restraint with height is approximately linear and roughly the same for all three cases. These restraints have been applied to both LRM and CPM for non-plane section analyses, and the maximum strain ratios are presented in table 1, where t is the time after casting.

Table 1 - CPM and LRM Results for example 1.

Case	Method	y, m	$t, h.$	Strain ratio, -
Case a	CPM	2.789	126	1.0500
	LRM	2.843	124	1.0143
	CPM-C	2.817	126	0.8051
	LRM-C	2.843	124	0.7363
Case b	CPM	2.873	116	0.9714
	LRM	2.843	130	1.0893
	CPM-C	2.873	116	0.9714
	LRM-C	2.843	130	1.0893
Case c	CPM	2.873	116	0.9714
	LRM	2.941	130	1.0369
	CPM-C	2.873	116	0.9714
	LRM-C	2.941	130	1.0369

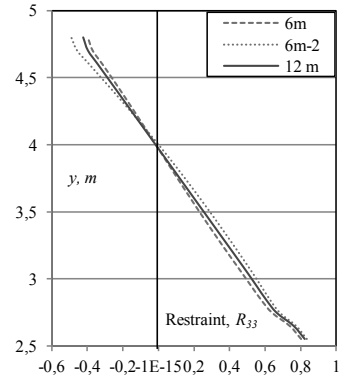


Figure 7 - Distribution of restraint with height in case a, b and c.

The denotation ‘-C’, see CPM-C and LRM-C, means that the slip factor according to figure 5 is taken into account. For the case a, the slip factor is 0.725, while in the other cases, b and c, there is no reduction due to slip effects, i.e. the slip factor is 1.0. The distributions of strain ratios at the time of maximum strain ratio are shown in figure 8. The strain ratio developments with time for the critical point are shown in figure 9. As can be seen in figure 8, the maximum strain ratios are approximately the same for case a using LRM and CPM, while the distribution in the wall is

somewhat different. For cases b and c, the distribution is roughly the same, but the maximum strain ratio differs by about ten percent. These deviations might be dependent on the L/H ratio. In figure 9, it can be seen that the curve shapes for the strain ratio vs. time in the critical positions are very similar using LRM and CPM.

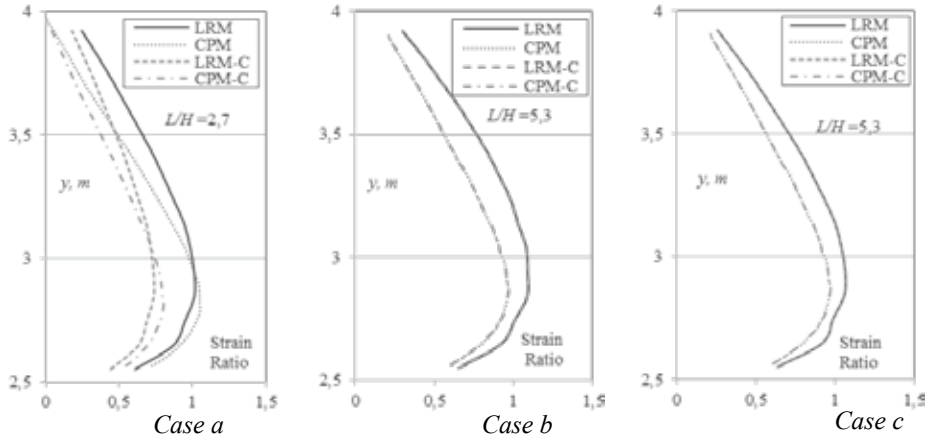


Figure 8 - Distribution of strain ratio with height at critical time using CPM and LRM.

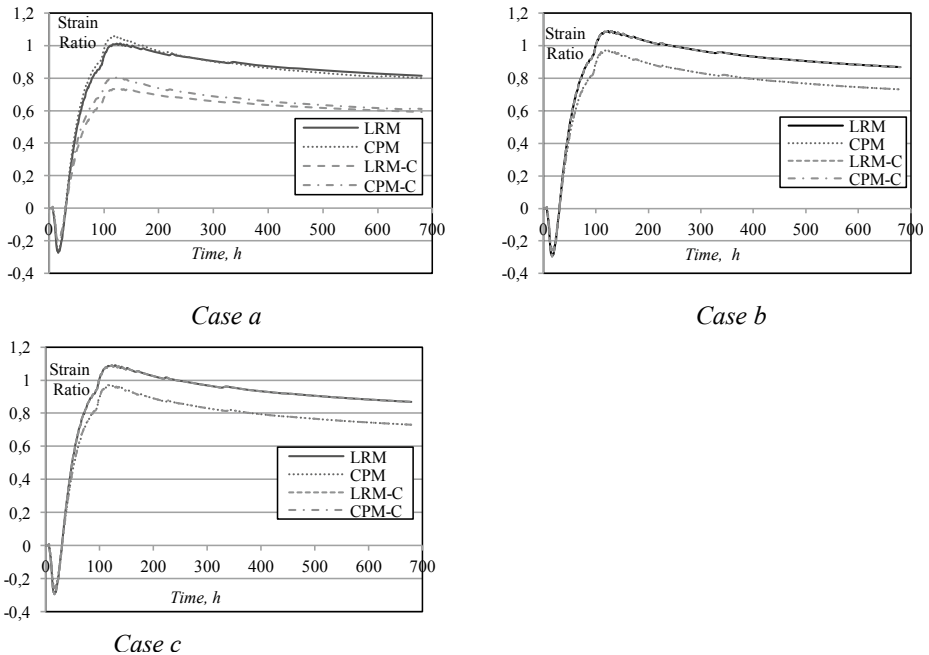


Figure 9 - Variation of strain ratio with time at the critical point in different casting situations, using CPM and LRM.

Example 2.

For a wall-on-slab structure, three walls with different length to height ratios are analyzed. The cross-section of the structure was constant; the width of the slab is 4m; the thickness of the slab

is 1m; the width of the wall is 1m; the height of the wall is 4m; and the length of the wall is 5m (L/H 1.25), 10m (L/H 2.5), and 15m (L/H 3.75), respectively. Different restraint conditions in the walls occur, which is seen in figure 10. As can be seen from the figure the distribution is highly non-linear in the short wall, $L=5m$, while the distribution is approximately linear for $L \geq 10m$.

The maximum strain ratios for the LRM and CPM are presented in table 2. For $L=5m$ and $L=10m$ the resulting strain ratio using CPM is larger than that using LRM. However, for $L=15m$ the strain ratio using CPM is smaller than that using LRM. Considering the results from both table 1 and table 2, it seems that both LRM and CPM results in approximately the same maximum strain ratio for L/H in the region of about 2-4. As the restraint curves are constructed with a uniform contraction in the young concrete, the calculations presented here correspond to the “natural” situation, i.e. without measures taken on site.

Further, for short structures (L/H less than about 2) CPM yields higher strain ratios than LRM, but for longer structures (L/H greater than about 4) the opposite applies. According to figure 5, all cases in example 2 have slip factors less than 1, which also can be seen in figures 11-16.

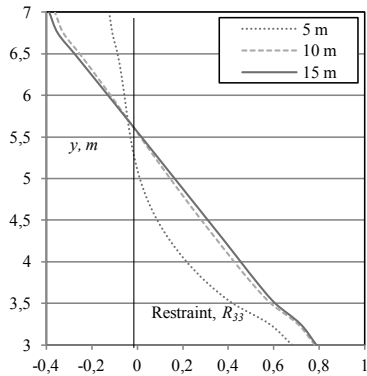


Figure 10 - Restraint variation with height for length 5, 10, and 15m.

Table 2 - CPM and LRM results for example 2.

Case	Method	y, m	t, h	Strain ratio, -
5m	CPM	3.325	272	1.3054
	LRM	3.25	272	1.0046
	CPM-C	3.325	272	0.7372
	LRM-C	3.25	272	0.5565
10 m	CPM	3.375	280	1.33
	LRM	3.5	272	1.2296
	CPM-C	3.375	280	1.0725
	LRM-C	3.5	272	0.97138
15 m	CPM	3.475	256	1.2428
	LRM	3.5	264	1.2719
	CPM-C	3.475	256	1.121
	LRM-C	3.5	264	1.157

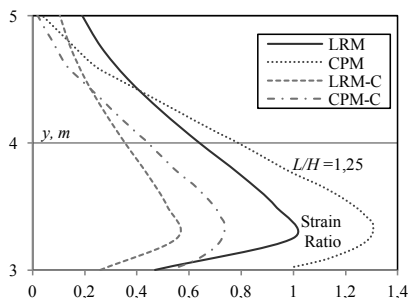


Figure 11 - Distribution of strain ratio with height at the critical time using CPM and LRM for 5m length.

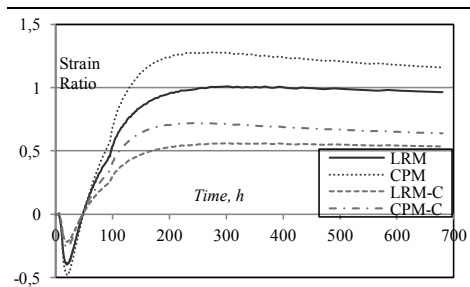


Figure 12 - Variation of strain ratio with time at the critical point for 5m length using CPM and LRM.

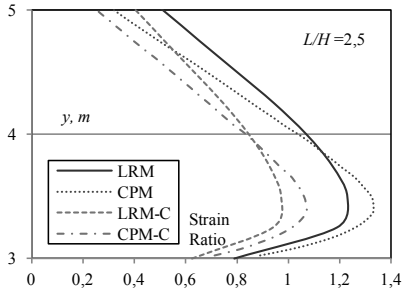


Figure 13 - Distribution of strain ratio with height, CPM and LRM using CPM and LRM for 10m

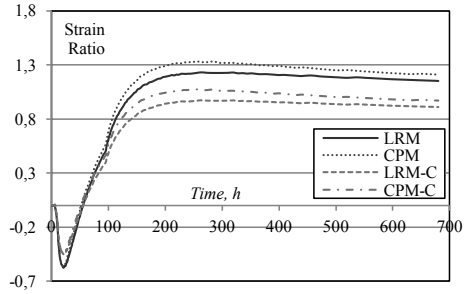


Figure 14 - Variation of strain ratio with time at the critical point using CPM and LRM for 10m

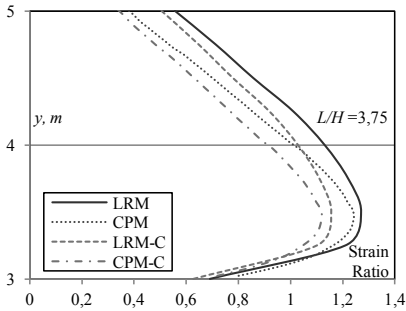


Figure 15 - Distribution of strain ratio with height, CPM and LRM for 15m length.

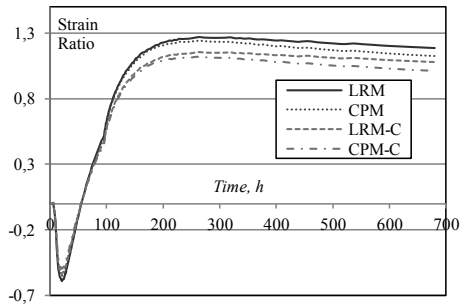


Figure 16 - Variation of strain ratio with time at the critical point using CPM and LRM for 15m.

Examples 1 and 2 show that CPM and LRM roughly give the same strain ratio distribution for L/H range approximately between 2 and 4. This is very interesting since CPM and LRM are based on simplifications of different types. In CPM the non-plane sectional analyses are accounted for by the reduction of the load using restraint factors for walls on stiff foundations (figure 2). In LRM the same restraint factor is applied from the very beginning, i.e. from the time of casting.

Tests and estimations in [26] showed a good agreement using CPM for $L/H = 2.7$ to 5.3 and in [27] for $L/H = 2.5$ to 5.1. From figures 8a and 8b with $L/H = 5.3$ it seems that LRM gives about 10% higher strain ratios than CPM. This indicates that LRM might give results on the safe side for L/H greater than about 4. In [25] it was shown that LRM agreed with observations for $L/H = 3$.

5.3 Development of equivalent restraint method ERM

The LRM can be used for analyzing the risk of through cracking when no measures are taken on site for situations where restraint curves have been established. The most common measures on site to reduce the crack risk are cooling of the newly cast concrete, [28] and [29], and heating of the adjacent structure [27]. CPM, when applicable, can be used for analysis and can accommodate both cooling and heating situations. As mentioned in chapter 4, basic LRM can only be used for cooling, if the estimated restraint is not changed significantly. In this chapter

the outline for an equivalent restraint method (ERM) is established. The aim of this method is that it may be applied to both cooling and heating situations. The main steps to outline the ERM are:

- 1) Establish a stress or strain curve in the young concrete taking into account the restraining from the adjoining structure without measures (cooling/heating) by using LRM.
- 2) Choose relevant parts of the young concrete and adjoining structures to be used in CPM. In most cases this means the use of the same cross-section as in LRM and a part of the adjoining structures.
- 3) Create an equivalent restraint model, ERM, by the use of CPM matching the stress or strain curves in step 1 for the critical part of the young concrete by adjustments of boundary conditions for the chosen structure in step 2. This is performed by adjusting the parameters R_M , R_N , δ_{res} in Figure 2 and δ_{slip} in figure 5.
- 4) ERM from step 3 can be applied to both cooling and heating with relevant interaction between old and young concrete in a similar way as in basic CPM.

In the outline of ERM above steps 2 and 3 are connected. This means that using a smaller part of the adjoining structure demands adjustments to higher restraint in step 3 than using a larger part of the adjoining structure. Reasonable choices of ERM structures for one example of a pillar on foundation slab are shown in section 5.4 below.

5.4 Example on application of ERM

The ERM is applied here to the second and third casting of the hollow pillar in figure 17. The first casting sequence could also be applied to ERM as well as basic CPM using the typical wall-on-slab structure, but this is not shown here. The dimensions of the slab are $1.7 \cdot 1.0$ m founded on frictional material. The outer dimension of the pillar is 3.8 m; the thickness of pillar walls is 0.5 m, and the height of each casting sequence of the pillar is 5 m.

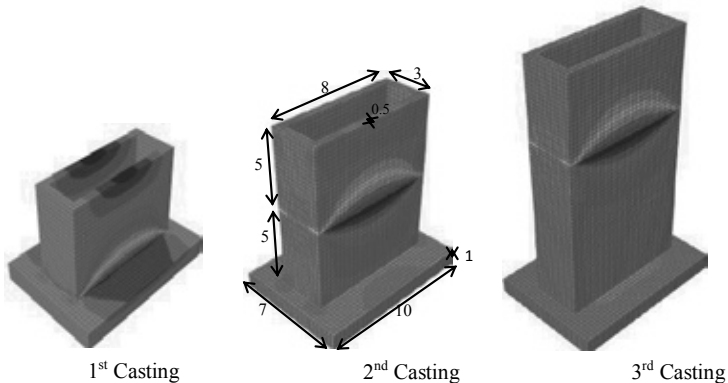


Figure 17 – Three casting sequence of a pillar.

Restraint curves from 3D calculations using Eq. 5 for homogeneous contraction in the new concrete are shown in Figure 18a for the first casting sequence of the pillar using different finite-element mesh from $0.05 \cdot 0.05$ m – $0.5 \cdot 0.5$ m. Based on these results the restraint curves in figure 18b are calculated using the mesh $0.25 \cdot 0.25$ m. As can be seen in the figure, the restraint curve is practically the same for sequences two and three, and the restraint for the first casting is somewhat higher.

The ERM is configured using CPM, where the new concrete and a chosen part of the adjacent old concrete is analyzed; see figure 19 for areas marked dark and light gray, respectively. For the ERM structure the boundary conditions are adjusted in such a way that the resulting stress-strain curve is in satisfactory agreement with the stress-strain ratios from LRM in the critical part of the young concrete, see LRM No measurement and EQM No measurement curves in figure 20. The construction of the ERM in figure 20 is created by the use of the ConTeSt program [15] with the following adjustments values: $R_M = 0$, $R_N = 0$, δ_{res} for $L=22m$, and $\delta_{slip}=0.95$.

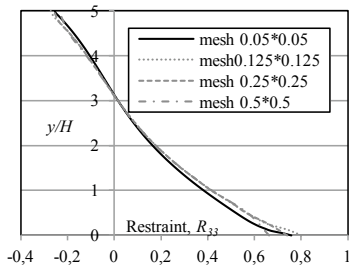


Figure 18a - Effect of mesh on restraint.

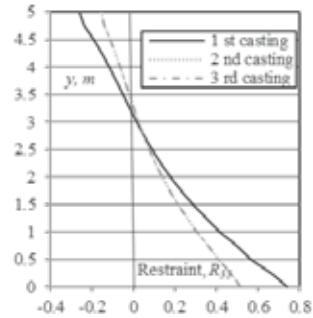


Figure 18b - Variation of restraint in three casting sequences of a pillar.

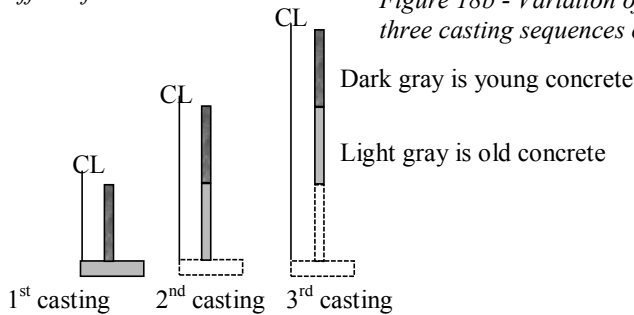


Figure 19 – Choice of equivalent models for three casting sequences of a pillar.

As can be seen in figure 20, the reduction of the strain ratio in the newly cast concrete can be estimated either by the LRM or the ERM for cooling in the young concrete or by the ERM when heating the adjacent structure before casting the new concrete .

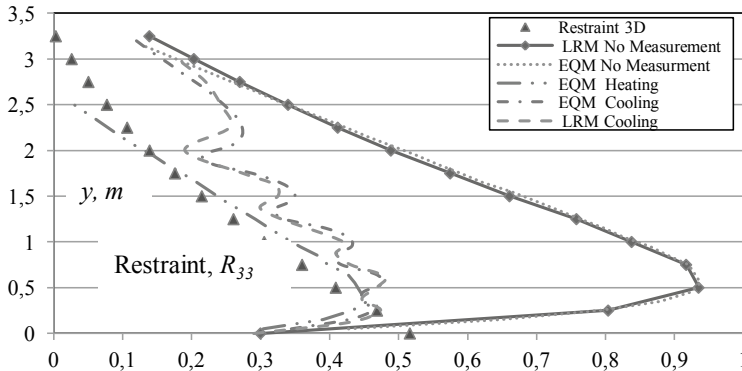


Figure 20 – Calibration of equivalent restraint method without measures, and effect of cooling pipes using LRM and ERM, and effect of heating using ERM.

6. RESTRAINT BY LRM FOR SOME COMMONLY USED INFRASTRUCTURES

6.1 General parameters

The restraint in the young concrete using Eq. 5 has been estimated in the 3D FEM calculations by the use of the following parameters:

- Elastic modulus in young concrete is 27.9 GPa.
- Elastic modulus in old (existing) concrete is 30 GPa.
- Poissons ratio in both young and old concrete is 0.2.
- Elastic modulus in rock is 20 GPa.
- Poissons ratio in rock is 0.35.

In the following, two specific infrastructures are used to show restraint curves for

- A double tunnel founded on frictional material
- A single tunnel founded on rock material

For the double tunnel the decisive restraints in different directions for consecutive casting sequences are calculated. For the single tunnel, the effect of different sizes of adjacent rock on the restraints in the length direction of the tunnel is presented.

6.2 Typical structure 1 - double tunnel founded on frictional material

The dimension and shape of the cross-section (in the xy plane) in the double tunnel is shown in figure 21. The length of each casting sequence is 15m (in the z direction).

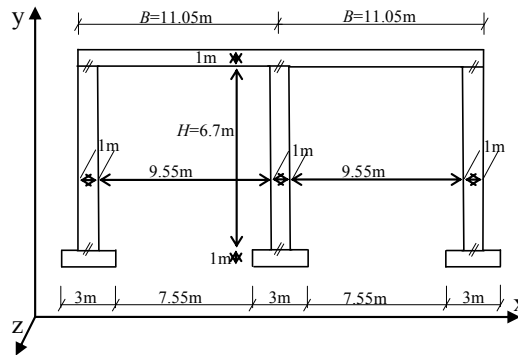


Figure 21- Cross-sectional dimensions of typical structure 1.

The restraint for typical structure 1 is estimated for three casting sequences for both walls and roofs, see figure 22. No restraint is estimated for the slabs as the dimensions are small and they are founded on frictional material. This means there is no significant risk of through cracking in the slabs.

All restraint curves are evaluated as uniaxial restraint parallel with the direction of the joint to the adjacent structure, see R_i in eq. 5. This means that for the walls R_{22} (R_y) and R_{33} (R_z) have been estimated depending on the direction of the restraining joint. For the roofs the corresponding restraints are R_{11} (R_x) and R_{33} (R_z) respectively.

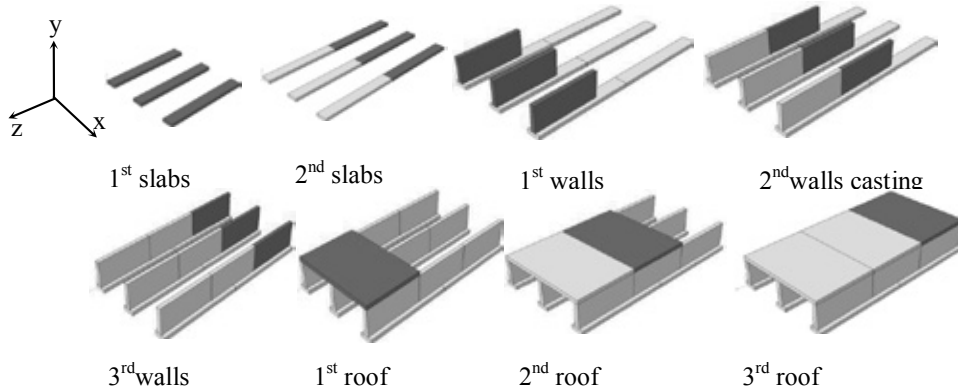


Figure 22 - Casting sequences for typical structure 1. Dark gray color means young concrete and light gray means old concrete.

The location of the maximum restraint in the horizontal joint between wall and slab for the 1st casting is at the middle of the joint, [13] and [16]. The resulting R_{33} in the critical point for typical structure 1 is shown in figure 23. For the 2nd and 3rd casting sequence of the wall, the critical point occurs at a distance of about $0.2L$ from the joint, [21] and [25]. The evaluated critical results are shown in figure 23. As can be seen in the figure, the restraints for the 2nd and 3rd castings are roughly the same. In the tensile region, from $y/H \approx 0.1$ to about 0.6 , the restraint for the 1st casting is somewhat lower than the restraints in the subsequent castings.

The location of the largest restraint in the vertical joint between wall and wall is about $0.2H$ from the joint. The resulting R_{22} in the critical point is shown in figure 24. The critical part, as regards cracking, is the tensile restraint region, in this case from $z/L = 0$ to about 0.2 . From figure 24 it is seen that the critical restraint is somewhat higher for the 3rd wall than in the 2nd wall casting.

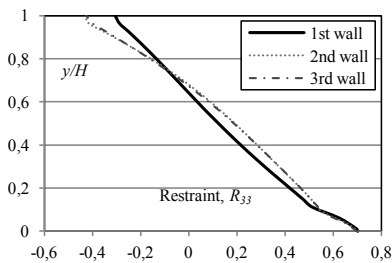


Figure 23- Restraint R_{33} in wall.

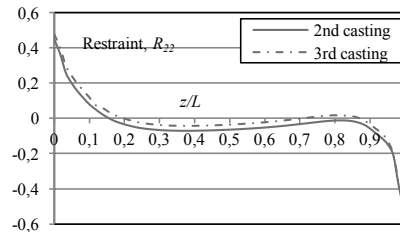


Figure 24 - Restraint R_{22} in wall.

For the 1st casting of the roof slab, the location of the largest restraint, as regards the horizontal joint between the roof and the wall, occurs in the middle of the roof in respect to the z -direction. The resulting R_{33} (R_Z) at the critical point is shown in figure 25. For the 2nd and 3rd castings of the wall, the critical point occurs near the outer walls at a distance of about $0.2L$ from the free edge (in the z -direction). The resulting R_{33} (R_Z) for $0.2L$ is shown in figure 25 and are denoted 2nd and 3rd roof. For the mid-section of the slab ($0.5L$) the largest restraints, R_{33} , occur near the inner walls and are higher than the corresponding restraints at $0.2L$ (compare the lines denoted 2nd and 3rd mid roof with those denoted 2nd and 3rd roof in figure 25). As can be seen in figure

25, the restraints in z-direction are different for all the casting sequences, and that the restraints are higher near the outer walls compared with the inner wall.

As regards the vertical joints between the different casting sequences of the roof, the location of the largest restraint occurs about $0.2B$ from the inner wall. The resulting R_{11} (R_X) at the critical point is shown in figure 26 for the 2nd and 3rd casting sequences. The rather small restraints for the 1st part of the roof are located at the position $z/L = 0.5$ and originate from the horizontal joints between the roof and the walls. The tensile restraint region for the 2nd and 3rd castings are rather large, from joint and up to about $0.7L$, and the restraints are roughly the same.

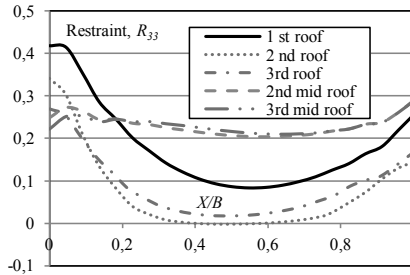


Figure 25 - Restraint R_{33} in the roofs.

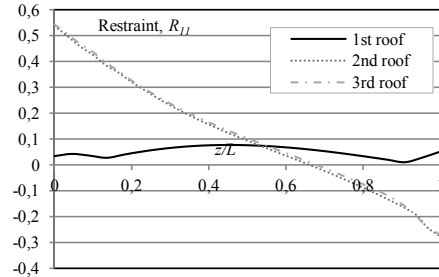


Figure 26 – Restraint R_{11} in the roofs.

6.3 Typical structure 2 - single tunnel founded on rock material

The shape of the cross-section (in the xy plane) for the single tunnel founded on rock and attached on two sides of the slabs (bottom and outer side), is shown in figure 27. Neither walls nor roof are connected to the rock. The length of each casting sequence is 17.5m (in the z direction). The restraint for typical structure 2 is estimated for two casting sequences for the slabs, walls and roofs, see figure 28.

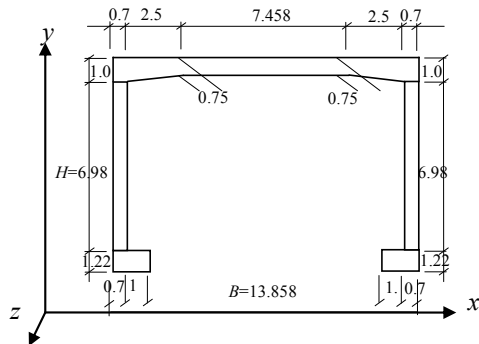


Figure 27- Cross-section of typical structure2.

All restraint curves are evaluated as R_{33} (R_Z) with respect to horizontal joints. The aim here is to evaluate the effect of rock dimensions on restraint in slabs, walls, and roof. The analyzed block of rock is shown in figure 29, where the side-length of the block, L_{Rock} , has been varied between 36 and 120m. The centre yz -cross-section is the same for the rock block and the concrete structure.

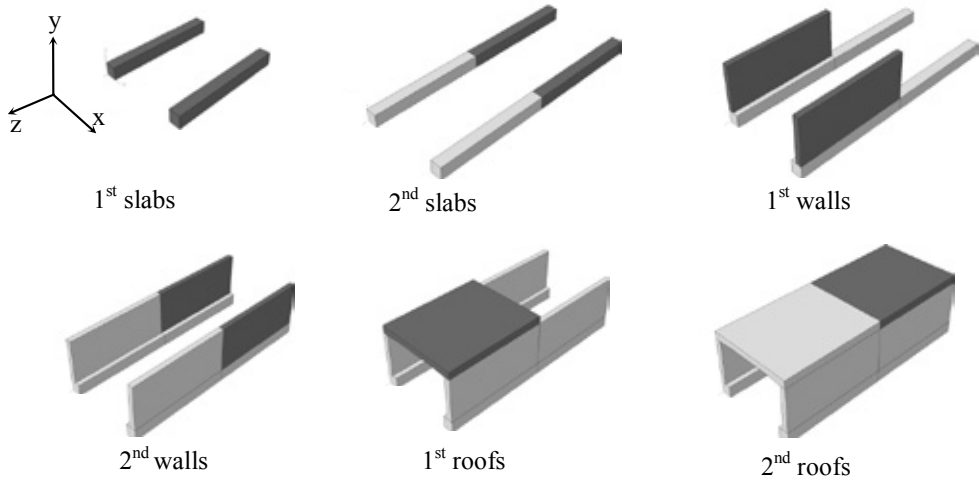


Figure 28 – Casting sequence of typical structure 2. Dark gray is young concrete, light gray is old.

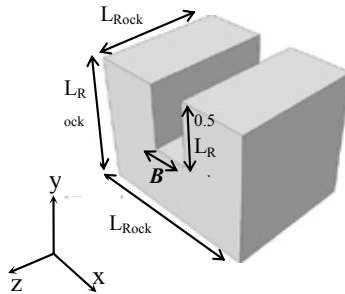


Figure 29 - Rock dimensions

For both the 1st and 2nd slab casting, the location of the largest R_{33} is in the middle of the slab. This result for the 1st slab is as expected, while this result for the 2nd slab is probably due to the effect of high restraint from the rock. As can be seen in figures 30 and 31, the restraint is higher in the 2nd slab, which probably originates from the horizontal joint between the slabs. The highest restraint is reached for rock blocks larger than 100m for the 1st slab casting, while for the 2nd slab casting it is already reached at L_{rock} equal to 50m.

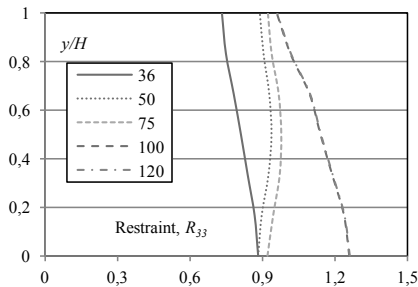


Figure 30 – Restraint R_{33} in 1st slab.

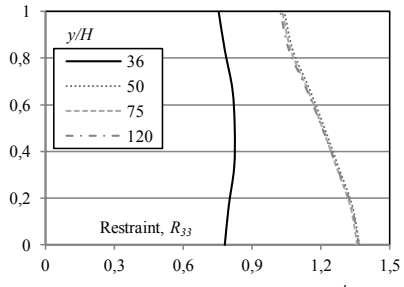


Figure 31 - Restraint R_{33} in 2nd slab.

The walls are not in contact with the rock at any position. The location of the largest restraint is in the middle of the wall for the 1st casting, and at about $0.25L$ from joint for the 2nd wall

casting. For both the 1st and 2nd roof casting the highest restraint effect is reached at a rock dimension of 50m, see figures 32 and 33. As can be seen in the figures, the restraint for the 1st roof casting is slightly lower than the 2nd roof casting.

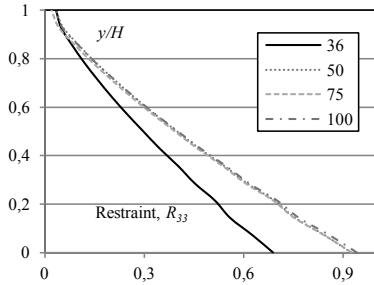


Figure 32 - Restraint R_{33} in 1st wall.

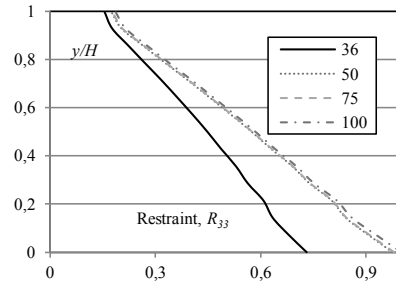


Figure 33 - Restraint R_{33} in 2nd wall.

For the 1st roof casting, the location of the largest restraint R_{33} is about $0.66L$ from the free edge, while the location of largest R_{33} in the 2nd roof casting is about $0.3L$ from the joint. The resulting R_{33} in the critical section is shown in figures 34 and 35. As can be seen from the figures, the highest restraint for both 1st and 2nd roof castings are reached at 50m. Figure 34 shows that the highest restraint is concentrated near the wall, while, on average, figure 35 shows somewhat higher restraint all over the roof in the critical section.

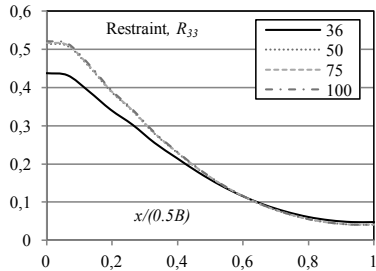


Figure 34 - Restraint R_{33} in 1st roof.

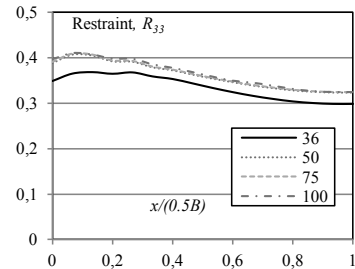


Figure 35 - Restraint R_{33} in 2nd roof.

The results for typical structures 1 and 2 might be applied directly in design (using LRM and ERM). It would be beneficial to study the effect of parameter variations to aid the implementation in practice.

Furthermore, it would be of interest to study other typical cases. In the second part [30] connected to this paper restraint factors for typical case wall-on-slab are presented in a simplified model using artificial neural network (ANN).

7. CONCLUSIONS

The CPM is primarily constructed to be used for structures with cross-sections simulated by axial deformation together with one or two rotations. This is not the case in more complicated structures, but LRM might be used in any type of structure at least as a basis for the estimation of risk for through cracking. Both CPM and LRM can be used when analyzing situations where no measures are taken on site. For walls-on-slabs CPM and LRM have shown to give resulting stresses for young concrete in the same order of size, especially for length to height ratios of about 2-4.

When CPM is applicable, measures taken on site, such as cooling and heating, are easy to examine, however when using basic LRM only cooling may be analyzed. In this paper an improved method, ERM (equivalent restraint method), has been developed. ERM is calibrated using LRM without measures, and it can easily be applied to accommodate both heating and cooling.

The restraint situations for two typical infrastructures are presented, and such restraint curves might be applied directly in design using LRM and ERM. For practical implementation it would be beneficial to perform further studies as regards the effects of parameter variation for a number of typical cases.

8. REFERENCES

1. ACI Committee 207, "Effect of Restraint, Volume Change, and Reinforcement on Cracking of Massive Concrete", ACI Committee 207.ACI207.2R-95. Reapproved 2002, 26 pp.
2. Emborg, M & Bernander, S., "Assessment of the Risk of Thermal Cracking in Hardening Concrete", *Journal of Structural Engineering*, ASCE, Vol.120, No 10, October 1994. pp. 2893-2912.
3. Mihashi, H., & Leite, J.P., "State of The Art Report on Control of Cracking in Early Age Concrete", *J. Advanced Concrete Technology*, 2004, 2 (2) pp. 141–154.
4. Kianousha, M.R., Acarcamb, M, Ziari, A., "Behavior of base restrained reinforced concrete walls under volumetric change", *Engineering Structures*, 30, 2008, pp. 1526–1534.
5. Cusson, D. & Repette, W., "Early-Age Cracking in Reconstructed Concrete Bridge Barrier Walls", *ACI Materials Journal*, 97(4), July/August, 2000, pp. 438-446.
6. Bosnjak, D., "Self-Induced Cracking Problems in Hardening Concrete Structures", Department of Structural Engineering, Norwegian University of Science and Technology Doctoral Thesis 2000, 171 pp.
7. Rostásy, F S, Tanabe, T., Laube, M., "Assessment of External Restraint. In: Prevention of Thermal Cracking in Concrete at Early Ages", Ed. by Springenschmid. London, England: E& FNSpon. RILEM Report 15. State of- the Art Report by RILEM Technical Committee 119, prevention of Thermal Cracking in Concrete at Early Ages.1998, pp. 149-177.
8. Emborg, M., "Development of Mechanical Behavior at Early Age", Ed. by R. Springenschmid. London, England: E & FNSpon. RILEM Report 15. State of- the Art Report by RILEM Technical Committee 119, Prevention of Thermal Cracking in Concrete at EarlyAges.1998, pp. 77-148.
9. JSCE, "English Version of Standard Specification for Concrete Structures 2007", Japan Society of Civil Engineer, JSCE, December, 2010, 503 pp.
10. Sato, R., Shimomura, T., Maruyama, I., Nakarai, K., "Durability Mechanics of Concrete and Concrete Structures Re-Definition and a New Approach", Committee Reports of JCI, 8th International Conference on Creep, Shrinkage and Durability of Concrete and Concrete Structures (CONCREEP8), Ise-Shima, Japan, 2008.10.1.
11. JCI., "A Proposal of a Method of Calculating Crack Width due to Thermal Stress", Tokyo, Japan: Japan Concrete Institute, Committee on Thermal Stress of Massive Concrete Structures, JCI Committee Report.1992, 106 pp.
12. Emborg, M., "Thermal Stresses in Concrete at Early Ages", Doctoral Thesis, Division of Structural Engineering, Lulea University of Technology, 1989, 172 pp.
13. Bernander, S., "Practical Measurement to Avoiding Early Age Thermal Cracking in Concrete Structures", Prevention of Thermal Cracking in Concrete at Early Ages. Ed.by R.

- Springenschmid. London, England: E & FNSpon. RILEM Report 15. State of- the Art Report by RILEM Technical Committee 119, prevention of Thermal Cracking in Concrete at Early Ages.1998, pp. 255-315.
14. Jonasson, J.E., Wallin, K., Emborg, M., Gram, A., Saleh, I., Nilsson, M., Larsson, M., Hedlund, H., "Temperature Cracks in Concrete: Manual With Diagrams Sprick risk bedömning Including Measures for Some Common Scenarios", Part D and E., Technical report / Lulea University of Technology, 2001:14. Lulea: Lulea University of Technology, 2001, 110 pp. (in Swedish).
 15. ConTeSt Pro., "User's Manual - Program for Temperature and Stress Calculations in Concrete", Developed by JEJMS Concrete AB in co-operation with Lulea University of Technology, Cementa AB and Peab AB. Lulea, Sweden, 2003, 198 pp.
 16. Nilsson, M., "Restraint Factors and Partial Coefficients for Crack Risk Analyses of Early Age Concrete Structures", Lulea, Sweden, Division of Structural Engineering, Lulea University of Technology. Doctoral Thesis 2003, 170 pp.
 17. Olofsson, J., "3D Structural Analyses of Crack Risk In Hardening Concrete Structures Verification of Three Steps Method Methods", Lulea University of Technology, Division of Structural Engineering, IPACS Report, ISBN 91-89580-53-2, 1999, 52 pp.
 18. Kheder, R., Al-Rawi, J., Al-Dhahi, K., "A Study of the Behavior of Volume Change Cracking in Base Restrained Concrete Walls", *Materials and Structures*, 27, 1994, pp. 383-392.
 19. Klemczak, B., & Knoppik, A., "Early Age Thermal and Shrinkage Cracks in Concrete Structures Influence of Geometry and Dimensions of Structure", *Architecture Civil Engineer Environment*, the Silesian University of Technology, No.3, 2011, pp. 55-62.
 20. Schiessl, P., Beckhaus, K., Schachinger, I., Rucker, P., "New Results on Early-Age Cracking Risk of Special Concrete", *Cement, Concrete and Aggregates*, Volume: 26, Issue Number: 2, 2004, ID CCA12304.
 21. Bamforth, P. B., "Early Age Thermal Crack Control in Concrete", CIRIA 2007, Construction Industry Research and Information Association, London, CIRIA 2007, RP722 ISBN 978-8-86107-660-2, 112 pp.
 22. Sule, M., & Van Breugel, K., "Cracking Behavior of Reinforced Concrete Subjected to Early-Age Shrinkage", *Materials and Structures*, Vol. 34, June 2001, pp. 284-292.
 23. 4C-Temp & Stress for concrete - Description. (n.d.), Retrieved from Danish Technological Institute: <http://www.dti.dk/1265>.
 24. B4cast ver. 3.0, User guide Available from ConTech Analysis ApS, program analyses <http://www.b4cast.com/default.htm>.
 25. Larson, M., "Thermal Crack Estimation in Early Age Concrete Models and Methods for Practical Application", Lulea, Sweden, Division of Structural Engineering, Lulea University of Technology, Doctoral Thesis 2003.
 26. Jonasson, J.E., Wallin, K., Nilsson, M., "Casting of Concrete Wall on Slabs, Study of Risk of Cracking Duo to Temperatures Changes during the Hardening Process", Lulea, Sweden, Division of Structural Engineering, Lulea University of Technology, 2009, 73 pp.
 27. Wallin, K., Emborg, M., Jonasson, J.E., "Heating Alternative to Cooling", Technical report, Lulea University of Technology, 1997:15.Lulea: Lulea University of Technology, 1997, 168 pp. (in Swedish).
 28. Emborg, M., & Bernander, S., "Avoiding of Early Age Thermal Cracking in Concrete Structures Predesign, Measures, Follow-Up", in "Thermal Cracking in Concrete at Early Ages", Proc. of the RILEM International Symposium, Edited by R. Springenschmid, E & FNSpon, London, 1994, pp. 409-416.
 29. COIN Project report no 31,Bjøntegaard, O., "Basis for Practical Approaches to Stress Calculations and Crack Risk Estimation in Hardening Concrete Structures, State of the

- Art”, (Norwegian Public Roads Administration), FA., 3, Technical performance, S.P., 3.1 Crack Free Concrete Structures, 2010, 142 pp.
30. Al-Gburi, M., Jonasson, J.E., Yousif, S., T., and Nilsson, M., “Simplified Methods for Crack Risk Analyses of Early Age Concrete Part 2: Restraint Factors for Typical Case Wall-on-Slab”, aim to be published in the Nordic Concrete Research as part 2 in connection to the present paper.

Simplified Methods for Crack Risk Analyses of Early Age Concrete Part 2: Restraint Factors for Typical Case Wall-on-Slab



Majid Al-Gburi
M.Sc. Ph.D. Student
Lulea University of Technology – Sweden
Dept. of Structural Engineering
Email: majid.al-gburi@ltu.se



Dr. Jan-Erik Jonasson
Professor
Lulea University of Technology – Sweden
Dept. of Structural Engineering
Email: jej@ltu.se



Dr. S. T. Yousif
Assistance professor
University of Mosul – Iraq
Email: styousif59112@yahoo.com



Dr. Martin Nilsson
Lulea University of Technology – Sweden
Email: martin.c.nilsson@ltu.se

ABSTRACT

Existing restraint curves have been applied to the method of artificial neural networks (ANN) to model restraint in the wall for the typical structure wall-on-slab. It has been proven that ANN is capable of modeling the restraint with good accuracy. The usage of the neural network has been demonstrated to give a clear picture of the relative importance of the input parameters. Further, it is shown that the results from the neural network can be represented by a series of basic weight and response functions. Thus, the results can easily be made available to any engineer without use of complicated software.

Key Words: Restraint curves, early age concrete, wall-on-slab, artificial neural network

1. INTRODUCTION

The main reason of stresses in young concrete is restraining of volume deformations caused by temperature and moisture changes at early ages [1]. Through cracking of the newly cast concrete is the most severe situation, as it occurs during the temperature contraction phase and as the crack remains open, see the position of the vertical dashed-dotted line in figure 1. To be able to realize estimations of through cracking the external restraint from adjacent structures needs to be known. Examples of calculation of restraint curves and how they are applied into estimations of risks for through cracking are shown in [2].

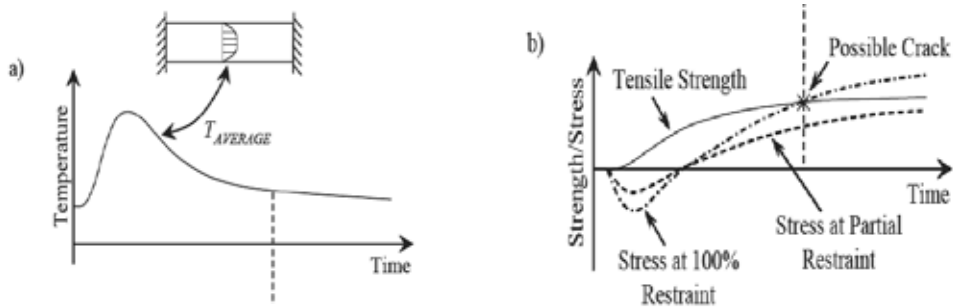


Figure 1 –Illustration of average temperature in young concrete and possible through cracking for different restraint conditions [1].

External restraint includes effects from adjacent structures like earlier casting sequences, foundations and subsoil. The degree of external restraint depends primarily on the relative dimensions and modulus of elasticity in the young concrete as well as in the surrounding restraining materials. The distribution of restraint varies at different positions of a concrete member [2].

The restraint in a section may be reduced in several ways, as for instance by favourable casting sequences or shortening the length of the section and suitable arrangements of construction joints. It is also possible to mitigate early age through cracking by the choice of a concrete mix with low temperature rise due to hydration or lower the casting temperature [3]. Most common measures on site is to cool the newly cast concrete or to heat the adjacent structure, [1] and [3].

When analyzing early age stresses in concrete based on restraint curves, we might use the local restraint method (LRM) or the equivalent restraint method (ERM) [2]. Without measures on site the application of LRM is obvious, and the measure cooling can be applied with both LRM and ERM, but heating can only be analyzed with ERM [2].

2. AIMS AND PURPOSES

The aims and purposes of this paper are to

- Apply and verify the use of artificial neural network for restraint curves concerning the typical structure wall-on-slab.
- Clarify the influences of geometrical dimensions on restraint in the wall.
- Develop a simplified method for practical application of the neural network for the typical case wall-on-slab.

3. ESTIMATION OF RESTRAINT IN EARLY AGE CONCRETE

In the literature there are many methods adopted to estimate and calculate the value of restraint in young concrete, see for example [4], [5], [6], [7] and [8]. Some of these methods need the use of a complex software, which usually is expensive and need experienced people.

In this study, an artificial neural network (ANN) is presented to calculate the amount of restraint in the wall for typical structure wall-on-slab. The analyzes are based on results from 2920 elastic finite element calculations of the restraint in the wall founded on a slab [1], where the geometrical dimensions of the wall and the slab are varied systematically within reasonable values. The resulting restraints are fed and verified by an ANN, and the outcome from ANN are transformed to an Excel spread sheet to make the estimation of restraints quick and easy to apply for any engineer. This saves both time and money at estimation of the restraint curve for walls founded on a slab.

3.1 Geometric effects on restraint for early age concrete

The degree of restraint depends on several factors, including geometry of structures, casting sequences, number and position of joints, and mechanical properties of materials. The effects from restraint are illustrated in the upper right part of figure 2 [3] as one essential part of a crack risk estimation for early age concrete.

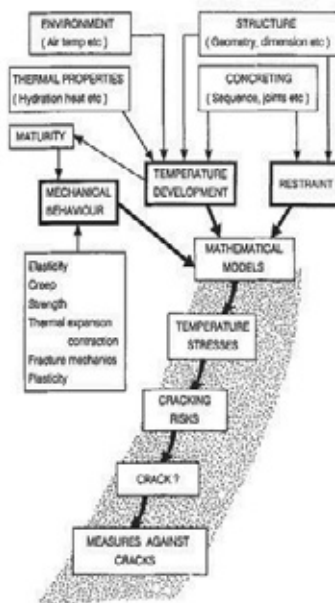


Figure 2 - Factors influencing stresses and cracking in early age concrete [3].

The restraint is reflected as a balance between the new concrete volume and the existing adjacent structure. In general, a larger volume of the new concrete results in a lower restraint while a small volume results in a high restraint, [9], [10] and [11].

The next chapter includes calculation of restraint in walls using the method of an artificial neural network based on geometric dimensions of the typical structure wall-on-slab.

4. APPLICATION OF THE ARTIFICIAL NEURAL NETWORK METHOD (ANN)

4.1 General overview

One form of artificial intelligence is the ANN, which attempts to mimic the function of the human brain and nerve system, but a simple unit of a neural network is much simpler than the biological cell [12].

A typical structure of ANN consists of a number of processing elements (PEs), or neurons, that usually are arranged in an input layer, an output layer and one or more hidden layers between, see figure 3 [13]. Each PE in a specific layer is fully or partially joined to many other PEs via weighted connections. The input from each PE in the previous layer (x_i) is multiplied by an adjustable connection weight (w_{ji}).

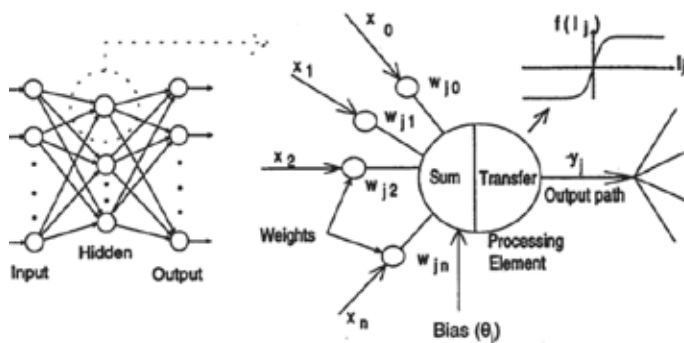


Figure 3 - Structure and operation of an ANN [13].

At each PE, the weighted input signals are summed and a threshold value or bias (θ_j) is added. This combined input (I_j) is then passed through a nonlinear transfer function, e.g. a sigmoid transfer function, to produce the output of the PEs (y_j). The output of one PE provides the input to the PEs in the next layer. This process is illustrated in figure 3, and explains in the next paragraph.

To determine the number of hidden neurons a network should have to perform its best, and one is often left out to the method of trial and error [14]. If the numbers of neurons are increased too much, over fit will occur, i.e. the net will have a problem to generalize. Each connection has a strength or weight that is used to modify the output of the neurons. The weights can be positive, which will tend to make the neuron go high, or negative, which will tend to make the neuron go low. The training process changes these weights to get the correct answers.

4.2 Learning an ANN

Artificial neural network models

Always we divide the data collected from field data or finite element programs in two groups. The first group is used in the training of the neural network (NN), and the other data group is used to test the obtained networks, Perceptron Multilayer (PML) networks, with a back-propagation algorithm used for the training. The multi-layer feed forward back-propagation technique is implemented to develop and train the neural network of current research, where the sigmoid transform function is adopted.

The Levenberg-Marquardt (LM) technique's built in MATLAB proved to be efficient training functions, and therefore, it is used to construct the NN model, [15] and [16]. This training function is one of the conjugate gradient algorithms that started the training by searching in the steepest descent direction (negative of the gradient) on the first iteration. The LM algorithm is known to be significantly faster than the more traditional gradient descent type algorithms for training neural networks. It is, in fact, mentioned as the fastest method for training moderately sized feed-forward neural network [14]. While each iteration of the LM algorithm tends to take longer time than each repetition of the other gradient descent algorithms, the LM algorithm yields far better results using little iteration, leading to a net saving in computer processor time. One concern, however, is that it may over fit the data. The network should be trained to recognize general characteristics rather than variations specific to the data set used for training.

Network data preparation

Pre-processing of data by scaling was carried out to improve the training of the neural network. To avoid the slow rate of learning near end points specifically of the output range due to the property of the sigmoid function, which is asymptotic to values 0 and 1, the input and output data were scaled between the interval 0.1 and 0.9. The linear scaling equation is expressed by:

$$y = \left(\frac{0.8}{\Delta} \right) X + \left(0.9 - \frac{0.8 X_{max}}{\Delta} \right) \quad (1)$$

Eq. 1 was used in this study for a variable limited to minimum (X_{min}) and maximum (X_{max}) values given in table 1, with:

$$\Delta = X_{max} - X_{min} \quad (2)$$

It should be noted that any new input data should be scaled before being presented to the network, and the corresponding predicted values should be un-scaled before use, [12] and [14].

Back propagation algorithm

The back propagation algorithm is used to train the BPNN (Back Propagation Neural Network). This algorithm looks for the minimum error function in weight space using the method of gradient descent. The combination of weights that minimizes the error function is considered to be a solution to the learning problem. The algorithm can be described in the following steps, [15] and [16]:

1. Once the input vector is presented to the input layer it calculates the input to the hidden layer, h_j^H , as:

$$h_j^H = \theta_j + \sum_{i=1}^{NI} w_{ji} x_i \quad (3)$$

where x_i represents the input parameter; θ_j represents the bias function of hidden layer; NI represent the number of neuron in the input layer; and w_{ji} represents the weight factor between input and hidden layer.

Each neuron of the hidden layer takes its input, h_j^H , and uses it as the argument for a function and produces an output, Y_j^H , given by:

$$Y_j^H = f(h_j^H) \quad (4)$$

2. Now the input to the neurons of the output layer, h_k^O , is calculated as:

$$h_k^O = \theta_k + \sum_{j=1}^{NH} w_{kj} Y_j^H \quad (5)$$

where θ_k represents the bias function of output layer; w_{kj} represents the weight factor between hidden and output layer; and NH represents the number of neuron in the hidden layer.

3. The network output, y_k , is then given by:

$$y_k = f(h_k^O) \quad (6)$$

where f represents the activation function.

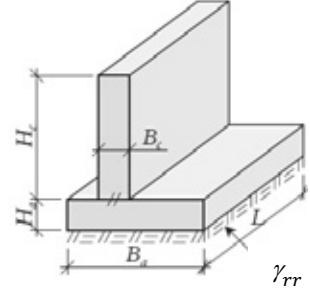
Training and testing of the neural networks

In [1] the geometry of 2920 wall-on-slab cases has been varied as shown in table 1. 2803 of them were used in the training of the neural network, as shown in figure 5a, and 117 were used for tests with the obtained network, as shown in figure 5b. Perception Multilayer (PML) networks, with a back-propagation algorithm, were used for the training. The multi-layer feed forward back-propagation technique is implemented to develop and train the neural network of current research, where the sigmoid transform function is adopted.

The training and testing results are given in figure 5 at the position $y/H_c = 0.1$, where y is the vertical co-ordinate above the upper surface of the slab. This height position is usually near the critical point at design with respect to the risk of through cracking in walls for typical structure wall-on-slab, [1] and [3]. As can be seen in the figure the coefficient of correlation, R , is 0.989 at training and 0.992 at verification, which indicates that the resulting model is very good.

Table 1 - List of parameters and their values used in the finite element method calculations of the elastic restraint variations in the walls of wall-on-slab structures [1].

Parameter	Sample	Maximum	Minimum	Unit
Slab width	B_a	8	2	m
Wall width	B_c	1.4	0.3	m
Slab thickness	H_a	1.8	0.4	m
Wall height	H_c	8	0.5	m
Length of the structure	L	18	3	m
External rotational restraint	γ_{rr}	1	0	-
Relative location* of the wall on slab	ω	1	0	-



*) $\omega = 0$ means a wall placed in the middle of the slab;
 $\omega = 1$ means a wall placed along the edge of the slab.

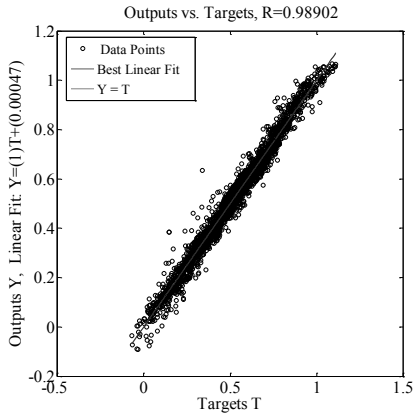


Figure 5a - Training results of ANN model at 0.1 wall height.

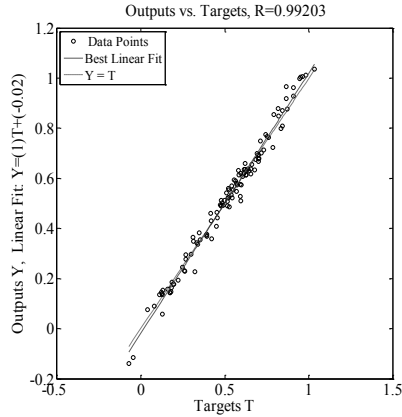


Figure 5b - Comparison between FEM-calculation and ANN model at 0.1 wall height.

5. STUDY OF IMPORTANCE GEOMETRY FACTORS MODEL

The method of the partitioning weights, proposed by Garson [17] and adopted by Goh [18], was used within this study in order to determine the relative importance of the various input parameters, see table 2. The major important parameter influencing the restraint is the wall height (H_c) at all levels of the wall (y/H_c) following by the external rotational restraint (γ_{rr}). The same indication is shown in [1]. Thereafter follow the wall thickness (B_c), and the length (L) of the structure. The relative location of the wall on the slab (ω) has a high impact in the lower part of the wall, and the effect decreases upward the wall. The thickness of the slab (H_a) has a little effect, and smallest influence has the width of the slab (B_a).

Table 2 - Relative importance on restraint of input parameters for wall-on-slab.

y/H_c	B_a	H_a	B_c	H_c	L	γ_{rr}	ω
0.0	4.65	12.61	19.62	18.63	5.85	17.85	20.76
0.1	6.97	11.84	17.7	20.11	11.24	20.44	11.66
0.2	7.3	13.6	14.14	21	11.68	15.65	16.63
0.3	6.8	11.0	11.6	26.2	12.4	16.8	15.2
0.4	8.89	12.87	12.47	21.47	12	16.6	15.68
0.5	7.68	10.15	12.9	25.57	15.36	13.37	14.56
0.6	6.66	8.04	11.36	29.84	16.46	21.15	6.47
0.7	5.99	9.75	10.9	30.97	16.41	19.12	6.82
0.8	6.73	7.44	9.61	32.1	14.95	23.16	5.98
0.9	6.36	5.36	8.01	42.23	13.67	18.9	5.43
1.0	4.13	4.42	8.01	41.6	23.15	14.67	3.97

6. STUDY OF PARAMETERS INFLUENCING THE RESTRAINT

In this chapter the restraints effects from different parameters are presented for the height $y = 0.1H_c$. Weight and threshold values for all heights, from $y=0$ to $y = H_c$, are shown in appendix A. In figures 6-11, the following symbols are used: $B_a = B_a$, $H_a = H_a$, $B_c = B_c$, $H_c = H_c$, $G_{rr} = \gamma_{rr}$ and $w = \omega$.

6.1 Effect of wall height (H_c)

The wall height is the most important factor affecting the degree of restraint in the case wall-on-slab, as shown in table 2. Generally, the degree of restraint decreases with an increase in wall height, which is compatible with the results shown in [1], [19], [20] and [21]. On the other hand, the restraint became bigger with increased wall length, as shown in figure 6, up to about 10m. Thereafter the restraint is no longer increasing with increased wall length.

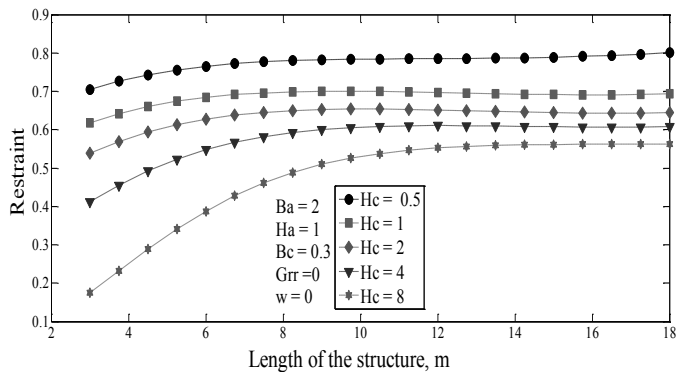


Figure 6 - Variation of restraint with length and wall height as predicted by ANN model at height $0.1 H_c$.

6.2 Effect of external rotational restraint (γ_{rr})

As shown in table 2, the second parameter of influence on restraint is the external rotational restraint. The bending moment during a contraction in a wall rotates the ends of the structure upward and the center downward. If the material under the foundation is stiff, the resistance on the structure is high, which at total rotational stiff ground reflects by γ_{rr} equal to 1. If the material under the foundations is very soft, the value of γ_{rr} is zero. The results of the ANN with $\gamma_{rr} = 1$ showed high restraint, which is in line with results in [22]. The restraint is about 40% lower when γ_{rr} is equal to zero. For both $\gamma_{rr} = 1$ and $\gamma_{rr} = 0$ the restraint increases with length of the structures up to about 10m (for $L/H_c \leq 5$), see figure 7.

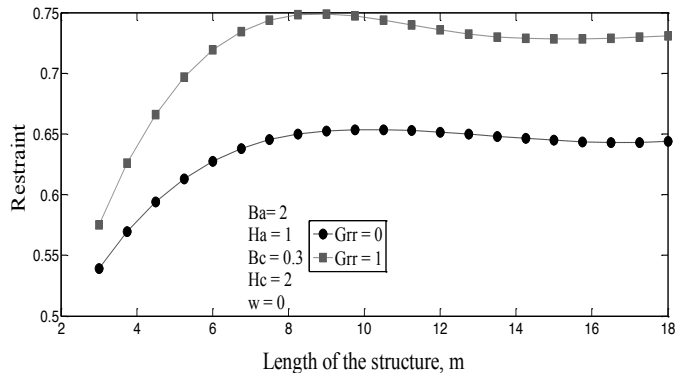


Figure 7 - Variation of the restraint with structural length and external rotational restraint as predicted by ANN model at height $0.1 H_c$.

6.3 Effect of wall thickness (B_c)

Increase of the size of the new concrete means higher possibility of counteracting the external constraints (from old concrete, i.e the slab in this case), which is reflected in figure 8 as the restraint will decrease with increased wall thickness. Besides, up to a structural length of 10m (for $L/H_c \leq 5$) the restraint increases with increased structure length, which is in agreement with results in [4], [23] and [24].

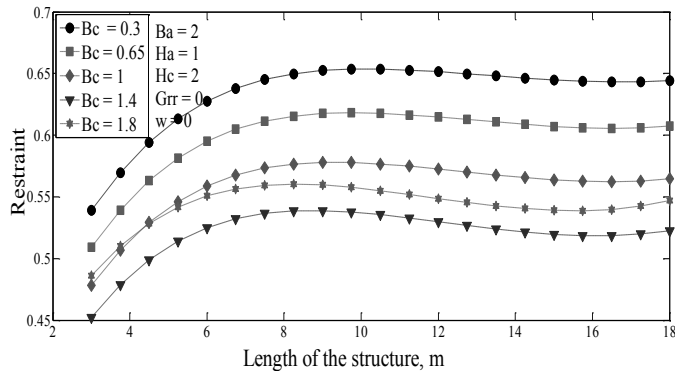


Figure 8 - Variation of the restraint with structural length and wall width as predicted by ANN model at height $0.1 H_c$.

6.4 Effect of the relative position of the wall on the slab (ω)

When a wall is placed in the middle of the slab ($\omega = 0$), it has the highest restraint from the slab, and other more eccentric positions become successively less and less restraint as shown in figure 9. An increase of the length of the structures results in increased restraint up to the length of about 10m (for $L/H_c \leq 5$).

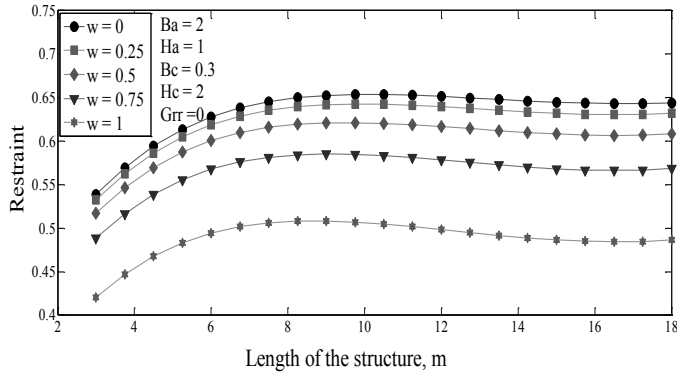


Figure 9 - Variation of the restraint with structural length and wall position on slab as predicted by ANN model at height $0.1 H_c$.

6.5 Effect of slab thickness (H_a)

An increase in slab thickness (H_a) results in an increased value of restraint. The effect of increasing the length of the wall is also increasing the value of restraint up to a length of about 10m (for $L/H_c \leq 5$), see figure 10. This is in agreement with findings in [4], [20], and [23].

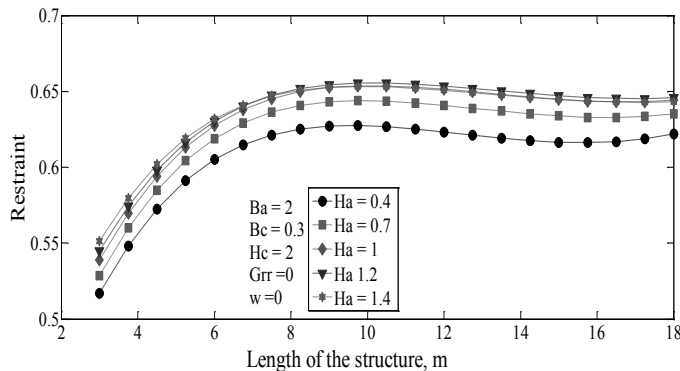


Figure 10 - Variation of the restraint with length and slab thickness as predicted by ANN model at height $0.1 H_c$.

6.6 Effect of slab width (B_a)

Generally, the value of restraint increases with the increase of the slab width for all levels of the wall height. A smaller increase in the value of restraint is observed with the increase in

structural length beyond 10m (for $L/H_c > 5$), see figure 11. The same indication is found in [4], [21], [25], and [26].

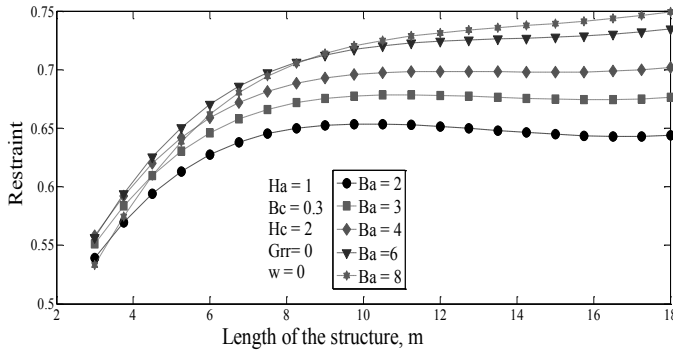


Figure 11 - Variation of the restraint with length and slab width as predicted by ANN model at height $0.1 H_c$.

7. ANN MODEL DEVELOPMENTS FOR RESTRAINT PREDICTION

The ANN model is used to derive a design formula to calculate the restraint by using multi-layer perceptions (MLP) for training the model with the back-propagation training algorithm. The model has seven inputs representing the width of the slab (B_a), the height of a slab (H_a), the width of the wall (B_c), the height of the wall (H_c), the length of the structure (L), the rotational boundary restraint (γ_{rr}), and the relative location of the wall on the slab (ω). All the parameters and their values are listed in table 1.

The structure of the optimal ANN model is shown in figure 12, while its connection weights and threshold levels are summarized in Appendix A, tables A1-A11.

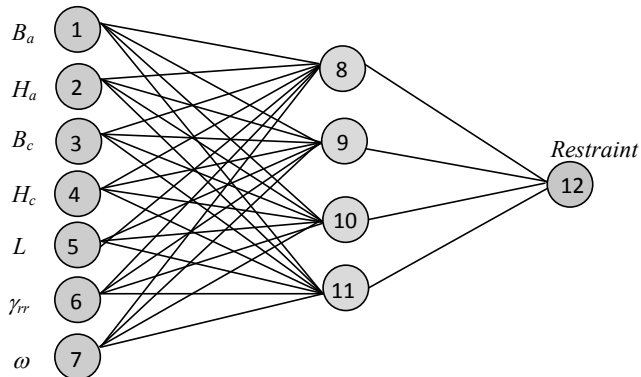


Figure 12 - Structure of the optimal ANN.

7.1 The design formula

The equation length depends on the number of nodes in the hidden layer. To shorten the length of the equation, an adoption of the number of nodes by four is introduced with a correctness of 95%. An adoption of 17 nodes gives an accuracy of 99%. The small number of connection weights of the neural network enables the ANN model to be translated into a relatively simple formula, in which the predicted restraint can be expressed as follows:

$$\gamma_R = \frac{1}{1+e^{-\left(\theta_{12} + \left(w_{8:12} \frac{1}{1+e^{-x_1}}\right) + \left(w_{9:12} \frac{1}{1+e^{-x_2}}\right) + \left(w_{10:12} \frac{1}{1+e^{-x_3}}\right) + \left(w_{11:12} \frac{1}{1+e^{-x_4}}\right)\right)}} \quad (7)$$

where

$$X_1 = \theta_8 + (w_{8:1}) \cdot (B_a) + (w_{8:2}) \cdot (H_a) + (w_{8:3}) \cdot (B_c) + (w_{8:4}) \cdot (H_a) + (w_{8:5}) \cdot (L) + (w_{8:6}) \cdot (\gamma_{rr}) + (w_{8:7}) \cdot (\omega) \quad (8)$$

$$X_2 = \theta_9 + (w_{9:1}) \cdot (B_a) + (w_{9:2}) \cdot (H_a) + (w_{9:3}) \cdot (B_c) + (w_{9:4}) \cdot (H_a) + (w_{9:5}) \cdot (L) + (w_{9:6}) \cdot (\gamma_{rr}) + (w_{9:7}) \cdot (\omega) \quad (9)$$

$$X_3 = \theta_{10} + (w_{10:1}) \cdot (B_a) + (w_{10:2}) \cdot (H_a) + (w_{10:3}) \cdot (B_c) + (w_{10:4}) \cdot (H_a) + (w_{10:5}) \cdot (L) + (w_{10:6}) \cdot (\gamma_{rr}) + (w_{10:7}) \cdot (\omega) \quad (10)$$

$$X_4 = \theta_{11} + (w_{11:1}) \cdot (B_a) + (w_{11:2}) \cdot (H_a) + (w_{11:3}) \cdot (B_c) + (w_{11:4}) \cdot (H_a) + (w_{11:5}) \cdot (L) + (w_{11:6}) \cdot (\gamma_{rr}) + (w_{11:7}) \cdot (\omega) \quad (11)$$

It should be noted that, before using Eqs. 7, 8, 9, 10, and 11, that all input variables need to be scaled between 0.1 and 0.9 using Eq. 1 for the data ranges in table 1. It should also be noted that predicted restraint obtained from Eq. 7 is scaled between 0.1 and 0.9 and in order to obtain the actual value, this restraint has to be re-un-scaled using Eq. 1. ANN should be used only for interpolation and not extrapolation [13].

7.2 Numerical example

A numerical example is provided to present the implementation of the restraint formula. Input parameters are: $B_a = 2\text{m}$, $H_a = 0.4\text{m}$, $B_c = 0.3\text{m}$, $H_c = 4\text{m}$, $L = 18\text{m}$, $\gamma_{rr} = 1$, and $\omega = 0$. As shown in figure 13, the convergence in results from finite-element (FE) calculations [1] and results using the Excel spread sheet is very good. Therefore, the Excel spread sheet can be used as a substitute for fast and accurate calculation of restraints in the wall.

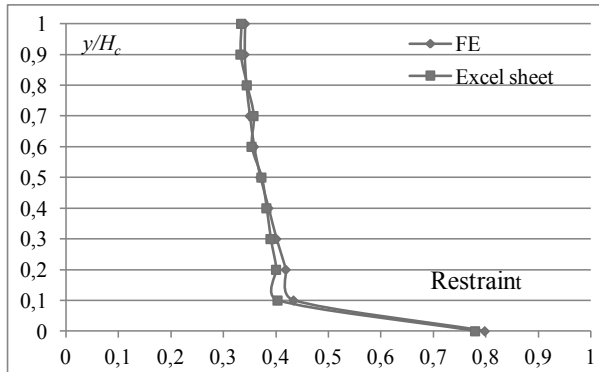


Figure 13- Comparison between finite-element restraints and results using the Excel spreadsheet.

8. CONCLUSIONS

Existing research concerning restraint curves has been applied to the method of artificial neural networks to model restraint in the wall for the typical structure wall-on-slab. Seven input parameters have been used, and it has been proven that the neural network is capable of modelling the restraint with good accuracy.

The usage of the neural network has been demonstrated to give a clear picture of the relative importance of the input parameters. The dimension of the wall (height and width) as well as the external rotational restraint turned out to give the highest importance on restraint in the wall. On the opposite, the width of the slab was found to be of least significance in this respect.

Further, it is shown that the results from the neural network can be represented by a series of basic weight and response functions. Resulting functions can easily be implemented to simple computer tools. Thus, the results can easily be made available to any engineer without use of complicated software.

REFERENCES

1. Nilsson, M., "Restraint Factors and Partial Coefficients for Crack Risk Analyses of Early Age Concrete Structures", Lulea, Sweden, Division of Structural Engineering, Lulea University of Technology, Doctoral Thesis 2003:19, 170 pp.
2. Al-Gburi, M., Jonasson, J.E., Nilsson, M., Hedlund, H., Hösthagen, A., "Simplified Methods for Crack Risk Analyses of Early Age Concrete Part 1: Development of Equivalent Restraint Method", aim to be published in the *Nordic Concrete Research* publication as part 1 in connection to the present paper.
3. Emborg, M., & Bernander, S., "Assessment of the Risk of Thermal Cracking in Hardening Concrete", *Journal of Structural Engineering (ASCE)*, Vol.120, No 10, October 1994, pp. 2893-2912.
4. ACI Committee 207, "Effect of Restraint, Volume Change, and Reinforcement on Cracking of Massive Concrete", ACI Committee 207.ACI207.2R-1995. Reapproved 2002, 26 pp.

5. JSCE, "English Version of Standard Specification for Concrete Structures 2007", *Japan Society of Civil Engineer*, JSCE, December 2010, 503 pp.
6. Cusson, D., & Hooegeveen, T., "An Experimental Approach for the Analysis of Early Age Behavior of High Performance Concrete Structures Under Restrained Shrinkage", *Cement and Concrete Research*, 2007, 37: 2, pp. 200-209.
7. Bamforth, P. B., "Early-age Thermal Crack Control in Concrete", CIRIA Report C660, Construction Industry Research and Information Association, London, 2007.
8. Olofsson, J., Bosnjak, D., Kanstad, T., "Crack Control of Hardening Concrete Structures Verification of Three Steps Engineering Methods", 2000, 13th Nordic Seminar on Computational Mechanics, Oslo.
9. Weiss, W. J., Yang, W., Shah, S. P., "Influence of Specimen Size/Geometry on Shrinkage Cracking of Rings", *Journal of Engineering Mechanics*, Vol. 126, No. 1, January, 2000, pp. 93-101.
10. Moon, J.H., Rajabipour, F., Pease, B., Weiss, J., "Quantifying the Influence of Specimen Geometry on the Results of the Restrained Ring Test", *Journal of ASTM International*, Vol. 3, No. 8, 2006, pp. 1-14.
11. Hossain, A.B., & Weiss, J., "The Role of Specimen Geometry and Boundary Conditions on Stress Development and Cracking in the Restrained Ring Test", *Cement and Concrete Research*, 36, 2006, pp. 189– 199.
12. Yousif, S. T., & Al-Jurmaa, M. A., "Modeling of Ultimate Load for R.C. Beams Strengthened with Carbon FRP using Artificial Neural Networks", *Al-Rafidain Engineering*, Vol.18, No.6, December 2010, pp. 28-41.
13. Shahin, M.A., Jaksa, M.B, Maier, H.R., "Artificial Neural Network–Based Settlement Prediction Formula for Shallow Foundations on Granular Soils", *Australian Geomechanics* September 2002, pp. 45-52.
14. Yousif, S. T., "Artificial Neural Network Modeling of Elasto-Plastic Plates", Ph.D. thesis, College of Engineering, Mosul University, Iraq, 2007, 198 pp.
15. Hudson B., Hagan, M., Demuth, H., "Neural Network Toolbox for Use with MATLAB", User's Guide, the Math works, 2012.
16. Hagan, M.T., Demuth, H.B., Beale, M.H., "Neural Network Design", Boston, MA: PWS Publishing, 1996.
17. Garson, G.D., "Interpreting Neural Network Connection Weights", *Artificial Intelligence*, Vol. 6, 1991, pp. 47-51.
18. Goh, A.T.C., "Back-Propagation Neural Networks for Modeling Complex Systems", *Artificial Intelligence in Engineering*, Vol.9, No.3, 1995, pp. 143-151.
19. Emborg M., "Thermal Stresses in Concrete Structures at Early Ages", Div. of Structural Engineering, Lulea University of Technology, Doctoral Thesis, 73D, 1989, 280 pp.
20. Kheder, G. F, Al-Rawi, R. S., Al-Dhahi, J. K., "A Study of the Behavior of Volume Change Cracking in Base Restrained Concrete Walls", *Materials and Structures*, 27, 1994, pp. 383-392.
21. Kheder, G.F., "A New Look at the Control of Volume Change Cracking of Base Restrained Concrete Walls", *ACI Structural Journal*, 94 (3), 1997, pp. 262-271.
22. Lin, F., Song, X., Gu, X., Peng, B., Yang, L., "Cracking Analysis of Massive Concrete Walls with Cracking Control Techniques", *Construction and Building Materials*, 31, 2012, pp. 12–21.
23. Kim S.C., "Effects of a Lift Height on the Thermal Cracking in Wall Structures", *KCI Concrete Journal* (Vol.12 No.1), 2000, pp. 47-56.
24. Larson M., "Evaluation of Restraint from Adjoining Structures", IPACS-Rep, Lulea University of Technology, Lulea, Sweden, 1999.

25. Nagy A. "Parameter Study of Thermal Cracking in HPC and NPC Structures", *Nordic Concrete Research*, No.26, 2001/1.
26. Kwak, H.G., & Ha, S.J., "Non-Structural Cracking in RC Walls: Part II. Quantitative Prediction Model", *Cement and Concrete Research* 36, 2006, pp. 761–775.

Appendix A

Weights and threshold levels for the ANN-model

Table A1: Weights and threshold levels for the ANN- model at 0.0 H_c

Hidden layer nodes	w_{ji} (weight from node at hidden layer i in the input layer to node j in the hidden layer)							Hidden threshold (θ_j)
	I=1	I=2	I=3	I=4	I=5	I=6	I=7	
I=8	-2.44	-0.133	1.92	1.56	1.75	-0.33	0.962	3.968
I=9	0.0448	0.4451	-3.90	0.805	0.386	-1.33	-8.569	-2.429
I=10	0.1464	4.28	-2.27	-1.08	-1.099	-2.75	-2.29	2.505
I=11	1.742	0.099	-1.800	-1.172	-0.813	0.4078	-0.738	5.5439
Output layer nodes	w_{ji} (weight from node i in the hidden layer to node j in the output layer)							Output Threshold (θ_j)
	I=8	I=9	I=10	I=11	-	-	-	
I=12	0.455	10.73	6.24	-0.4758				-4.88

Table A2: Weights and threshold levels for the ANN- model at 0.1 H_c

Hidden layer nodes	w_{ji} (weight from node hidden layer i in the input layer to node j in the hidden layer)							Hidden threshold (θ_j)
	I=1	I=2	I=3	I=4	I=5	I=6	I=7	
I=8	0.0228	0.21462	0.3629	-18.48	0.9613	1.122	0.212	-2.271
I=9	0.422025	-0.06176	1.98924	-0.6882	0.30437	-0.26	-0.417	-1.2636
I=10	0.456249	0.983905	0.64158	0.13169	0.3093	-0.68	-0.168	-0.3123
I=11	0.238852	0.70202	-0.7221	0.60450	0.18516	-0.41	0.0307	-0.334
Output layer nodes	w_{ji} (weight from node i in the hidden layer to node j in the output layer)							Output Threshold (θ_j)
	I=8	I=9	I=10	I=11	-	-	-	
I=12	9.014351	-12.8866	15.6198	-21.768				5.60494

Table A3: Weights and threshold levels for the ANN - model at 0.2 H_c

Hidden layer nodes	w_{ji} (weight from node hidden layer i in the input layer to node j in the hidden layer)							Hidden threshold (θ_j)
	I=1	I=2	I=3	I=4	I=5	I=6	I=7	
I=8	0.023445	0.21469	0.361232	-18.5183	0.96787	1.12751	0.21163	-2.24292
I=9	-0.42725	-0.2689	0.31187	-0.70018	2.02201	-0.06425	0.431046	-1.28285
I=10	-0.1732	-0.7011	0.317028	0.129956	0.66889	1.008782	0.469116	-0.32013
I=11	0.03241	-0.4146	0.18831	0.61946	-0.7446	0.71167	0.24299	-0.33843
output layer nodes	w_{ji} (weight from node i in the hidden layer to node j in the output layer)							Output threshold (θ_j)
	I=8	I=9	I=10	I=11	-	-	-	
I=12	8.7721	-12.329	14.5275	-20.611				5.428395

Table A4: Weights and threshold levels for the ANN- model at 0.3 H_c

Hidden layer nodes	w_{ji} (weight from node hidden layer i in the input layer to node j in the hidden layer)							Hidden threshold (θ_j)
	I=1	I=2	I=3	I=4	I=5	I=6	I=7	
I=8	0.02282	0.2146	0.36293	-18.4809	0.96137	1.122909	0.212814	-2.27106
I=9	-0.41754	-0.2642	0.30437	-0.68824	1.98924	-0.06176	0.42202	-1.26363
I=10	-0.16823	-0.6808	0.30936	0.13169	0.64158	0.98390	0.45624	-0.31232
I=11	0.030785	-0.4095	0.185169	0.604506	-0.7221	0.707202	0.23885	-0.33428
Output layer nodes	w_{ji} (weight from node i in the hidden layer to node j in the output layer)							Output threshold (θ_j)
I=8	I=9	I=10	I=11	-	-	-	-	
I=12	9.014351	-12.886	15.61978	-21.7685				5.60494

Table A5: Weights and threshold levels for the ANN - model at 0.4 H_c

Hidden layer nodes	w_{ji} (weight from node hidden layer i in the input layer to node j in the hidden layer)							Hidden threshold (θ_j)
	I=1	I=2	I=3	I=4	I=5	I=6	I=7	
I=8	2.08677	1.89426	-13.088	-1.1256	-0.8407	41.17545	-32.701	-6.50761
I=9	0.377159	0.839513	-0.18151	-20.125	-0.3396	1.031952	-0.6816	1.04641
I=10	0.562324	0.737864	-0.90535	-1.2830	-0.6673	0.518905	-0.4199	-1.09078
I=11	0.579971	0.730745	-0.7001	-0.1999	-2.6483	0.734031	-0.4312	-2.35647
Output layer nodes	w_{ji} (weight from node i in the hidden layer to node j in the output layer)							Output threshold (θ_j)
I=8	I=9	I=10	I=11	-	-	-	-	
I=12	0.419494	2.097828	9.638326	-18.157				-1.666

Table A6: Weights and threshold levels for the ANN - model at 0.5 H_c

Hidden layer nodes	w_{ji} (weight from node hidden layer i in the input layer to node j in the hidden layer)							Hidden threshold (θ_j)
	I=1	I=2	I=3	I=4	I=5	I=6	I=7	
I=8	-1.45824	-2.32771	0.962872	-8.541	17.20482	22.46012	0.418163	-19.6627
I=9	0.756076	1.319794	-1.30934	-15.31	1.05319	0.74600	-0.42114	0.208142
I=10	-0.76824	0.25679	-0.64332	-8.505	9.60673	-4.05398	-0.69526	1.556513
I=11	1.10672	1.1844	-1.2012	0.3616	-2.586	-1.3277	-1.460	4.105541
Output layer nodes	w_{ji} (weight from node i in the hidden layer to node j in the output layer)							Output threshold (θ_j)
I=8	I=9	I=10	I=11	-	-	-	-	
I=12	1.38328	2.76767	0.91604	2.4217				-4.05196

Table A7: Weights and threshold levels for the ANN -model at 0.6 H_c

Hidden layer nodes	w_{ji} (weight from node hidden layer i in the input layer to node j in the hidden layer)							Hidden threshold (θ_j)
	I=1	I=2	I=3	I=4	I=5	I=6	I=7	
I=8	0.62026	0.47351	0.08976	5.18154	-3.78167	0.3101	-0.35249	1.50859
I=9	0.164556	1.471751	0.243077	23.6184	-24.3285	-32.39	1.23612	27.6750
I=10	-0.3054	-0.06287	-0.51847	-5.7015	3.504167	-0.065	0.054154	-1.11537
I=11	0.3387	1.058383	-0.44985	-27.486	0.912928	-0.366	-0.07223	1.450579
Output layer nodes	w_{ji} (weight from node i in the hidden layer to node j in the output layer)							Output threshold (θ_j)
I=8	I=9	I=10	I=11	-	-	-	-	
I=12	10.75089	-0.92821	11.19475	2.29642				-11.3610

Table A8: Weights and threshold levels for the ANN -model at 0.7 H_c

Hidden layer nodes	w_{ji} (weight from node hidden layer i in the input layer to node j in the hidden layer)							Hidden threshold (θ_j)
	I=1	I=2	I=3	I=4	I=5	I=6	I=7	
I=8	0.42400	0.46559	-0.1034	5.27938	-4.29611	0.05693	-0.223	1.94446
I=9	0.20791	0.18420	0.20273	5.76087	-4.2182	-0.5358	-0.031	1.80288
I=10	0.65041	2.65318	-1.61066	-38.5765	1.52342	-7.6225	0.2018	3.22180
I=11	0.111222	0.213763	-0.64653	-38.1758	2.497382	9.53468	-0.973	-4.43226
Output layer nodes	w_{ji} (weight from node i in the hidden layer to node j in the output layer)							Output threshold (θ_j)
	I=8	I=9	I=10	I=11	-	-	-	
I=12	14.2932	-14.2761	1.782392	1.422751	-	-	-	-1.32971

Table A9: Weights and threshold levels for the ANN -model at 0.8 H_c

Hidden layer nodes	w_{ji} (weight from node hidden layer i in the input layer to node j in the hidden layer)							Hidden threshold (θ_j)
	I=1	I=2	I=3	I=4	I=5	I=6	I=7	
I=8	0.482716	1.208346	-0.4909	5.799786	-4.74126	2.507117	-0.529	0.186043
I=9	0.715349	0.563623	0.37424	38.31441	-19.5478	-1.05955	-0.063	-1.96305
I=10	0.757585	1.53234	-1.3743	-17.3411	2.203233	-3.26635	-0.051	-0.26653
I=11	0.579219	0.284736	-1.1736	-11.4707	4.159462	7.178042	-0.853	-6.87323
Output layer nodes	w_{ji} (weight from node i in the hidden layer to node j in the output layer)							Output threshold (θ_j)
	I=8	I=9	I=10	I=11	-	-	-	
I=12	2.574084	-1.41622	4.10681	2.846912	-	-	-	-2.155

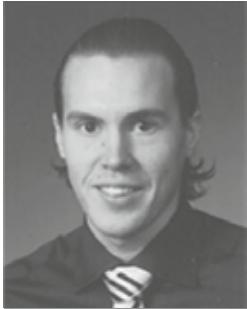
Table A10: Weights and threshold levels for the ANN- model at 0.9 H_c

Hidden layer nodes	w_{ji} (weight from node hidden layer i in the input layer to node j in the hidden layer)							Hidden Threshold (θ_j)
	I=1	I=2	I=3	I=4	I=5	I=6	I=7	
I=8	0.23413	0.39783	-0.1258	4.48423	-2.73151	0.31317	-0.11	0.838376
I=9	-0.72798	-2.68067	1.4830	30.1924	-0.56191	4.97414	-0.445	-2.30485
I=10	0.117852	0.00236	-0.2931	-7.23425	1.47341	0.96875	-0.165	0.709421
I=11	-0.01498	-0.12181	-0.1528	-5.9498	2.101039	0.556965	-0.072	-0.16348
Output layer nodes	w_{ji} (weight from node i in the hidden layer to node j in the output layer)							Output Threshold (θ_j)
	I=8	I=9	I=10	I=11	-	-	-	
I=12	19.49644	-1.96336	-16.522	36.35604	-	-	-	-18.3594

Table A11: Weights and threshold levels for the ANN- model at 1 H_c

Hidden layer nodes	w_{ji} (weight from node hidden layer i in the input layer to node j in the hidden layer)							Hidden layer threshold (θ_j)
	I=1	I=2	I=3	I=4	I=5	I=6	I=7	
I=8	0.10182	0.66933	-9.45E-	4.53729	-3.77808	3.23152	-0.0659	0.35271
I=9	0.206039	0.070818	0.26018	21.02211	-6.83813	-0.35579	0.14037	-2.78455
I=10	-0.10211	0.271457	-0.1774	-26.613	4.154443	0.310213	-0.0372	5.312146
I=11	0.422038	0.611063	-0.7748	-8.54489	1.897913	-0.74841	-0.1359	-1.07541
Output layer nodes	w_{ji} (weight from node i in the hidden layer to node j in the output layer)							Output threshold (θ_j)
	I=8	I=9	I=10	I=11	-	-	-	
I=12	4.860535	-4.40516	-3.2183	8.698041	-	-	-	-1.1289

Transversal Post Tensioning of RC Trough Bridges – Laboratory Tests



Jonny Nilimaa
M.Sc., Ph.D. Student
Luleå University of Technology
Dept. of Structural Engineering
SE – 971 87 Luleå
E-mail: jonny.nilimaa@ltu.se



Dr. Thomas Blanksvärd
Associate Senior Lecturer
Luleå University of Technology
Dept. of Structural Engineering
SE – 971 87 Luleå
E-mail: thomas.blanksvard@ltu.se



Dr. Lennart Elfgren
Professor
Luleå University of Technology
Dept. of Structural Engineering
SE – 971 87 Luleå
E-mail: lennart.elfgren@ltu.se



Dr. Björn Täljsten
Professor
Luleå University of Technology
Dept. of Structural Engineering
SE – 971 87 Luleå
E-mail: bjorn.taljsten@ltu.se

ABSTRACT

The Swedish Transport Administration (Trafikverket) is the owner of a large number of railway concrete trough bridges, which were designed according to Swedish design codes in the 1950's. The traffic loads are today higher than the design loads and the horizontal level of ballast is also much higher today, which implies that the contribution from the ballast to the deadload is considerable. The degree of utilization of the bottom slab is very high, which can be confirmed by calculations and visual inspections (flexural cracks are visible). This paper presents the results from a laboratory test on scaled down trough bridge specimens strengthened by transversal post-tensioning of the slab.

Calculations according to two design codes where the horizontal prestressing force is considered, gives a theoretical increase of the shear capacity with 5 – 11%, and the test indicated an even larger

increase of shear capacity. The main objective for the strengthening was to increase the shear capacity. In addition, adding a prestressing force also increased the theoretical flexural capacity, in this case with 21%.

Key Words: Strengthening, Post-Tensioning, Prestress, Retrofit, Trough bridge, Concrete, Upgrade

1. INTRODUCTION

There are approximately 300,000 railway bridges in Europe and about two thirds of them are more than 50 years old [1]. In general, as a bridge grow older, deterioration will affect the performance level, and this often occurs in combination with changes in structural requirements and demands. The society is constantly evolving, forcing the infrastructure to manage all kinds of changes. The railway system is also striving to increase traffic intensities, -loads, and -velocities, while design criteria and design codes are changing along with new research findings. Eventually, all bridges will reach a point when they can no longer provide a required safety margin for the users, i.e. it is no longer safe to use the bridge in the present state.

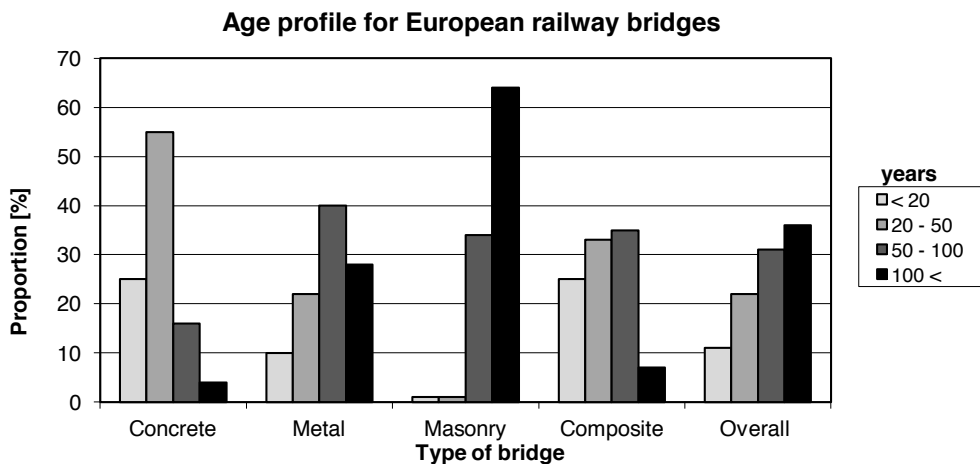


Figure 1 – Age profile for European railway bridges.

When such a situation occurs, the bridge owner will need to make a difficult decision about how to handle the structure. The first step is always to do an assessment of the existing structure. Sometimes it might be possible to upgrade the performance level only by executing new calculations according to the present standards, e.g. administrative upgrading. In this paper the following definitions are used; maintenance is defined as an action to keep the present performance level (lower than the original level), repair brings up the level of performance to its original state and upgrading increases the performance above its original state. Performance is often referred to increased load carrying capacity, but could also concern deterioration, function or aesthetic appearance. In this paper upgrading refer to increased load carrying capacity, but in cases when a bridge cannot be upgraded without any physical measures, there are three possible alternatives for the bridge owner;

- 1) Keep using the existing structure, but with reduced capacity and if necessary monitor.
- 2) Strengthening of the existing structure, to increase the load carrying capacity.
- 3) Replacing of the existing structure with a new one that fulfils the demands.

In some cases it might be possible to continue using the old structure with a reduction in the capacity. But if the objective is to e.g. increase the performance, this might not be a satisfying alternative. There are many ways to strengthen a bridge and current research is constantly developing new methods, e.g. [2], [3], but it is not always economically or physically viable to strengthen all old structures, some of them require to be replaced.

The Swedish Transport Administration (Trafikverket) is the owner of a large number of railway concrete trough bridges, which were designed according to standard codes in the 1950's. The traffic loads are today higher than the original design loads and the level of ballast is also much higher today. The degree of utilization of the bottom slab is very high, which can be confirmed by calculations and visual inspections (flexural cracks are in many objects visible). Several methods for flexural strengthening of trough bridges have been tested and are well documented, e.g. [4], [5], but there is a lack of strengthening methods, applicable for shear strengthening of bridges in-situ. The objective of this paper is to investigate the possibility to strengthen trough bridges by transversal post-tensioning and the strengthening effects on the shear capacity.

2. METHOD

2.1 Experimental program

Two specimens (B1 & B2) were tested in order to investigate the possibility to strengthen RC trough bridges by transversal post-tensioning with internal unbonded steel tendons and the effects on the structural behavior of such a strengthening system. The specimens were designed in resemblance to the design drawings of existing railway trough bridges from the 1950's, but reduced to a scale of 1/3. B1 was unstrengthened and used as a reference specimen, while B2 was strengthened by three transversal post-tensioned unbonded internal steel tendons, denoted N in Figure 2.

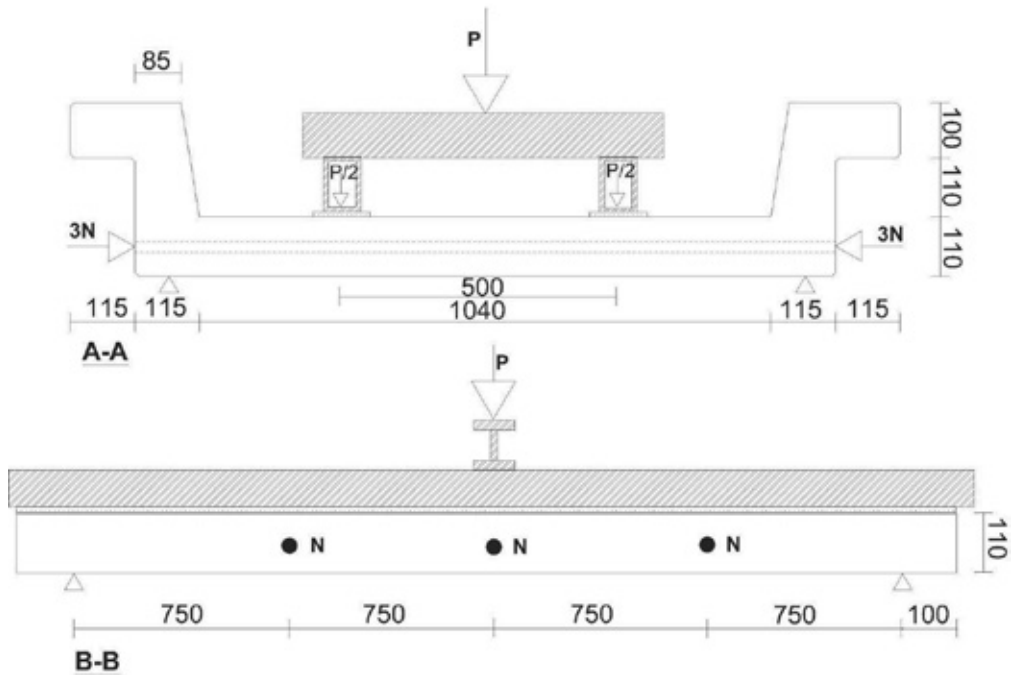


Figure 2 – Test setup, cross sectional view, in [mm].

2.2 Test setup

Geometry

The length of the specimen was 1700 mm, the width was 1500 mm (including main girders), the thickness of the slab was 110 mm and the height of the girders was 220 mm. Geometrical data for the test specimen are illustrated in Figures 2 and 3. The internal reinforcement consisted of deformed steel bars with diameters of 6, 8 and 10 mm. Compressive and tensile reinforcement were located at 23 and 86 mm, with internal spacing of 150 and 120 mm, respectively. The strengthening system included three steel tendons, located at mid height of the bottom slab, as shown in Figure 2.

Supports

The specimens were arranged on top of four semi spherical steel supports, one in each corner, as illustrated in Figure 2. Normally a trough bridge would be supported along two opposite sides, but since the aim was to investigate the transversal behavior, the present approach was chosen.

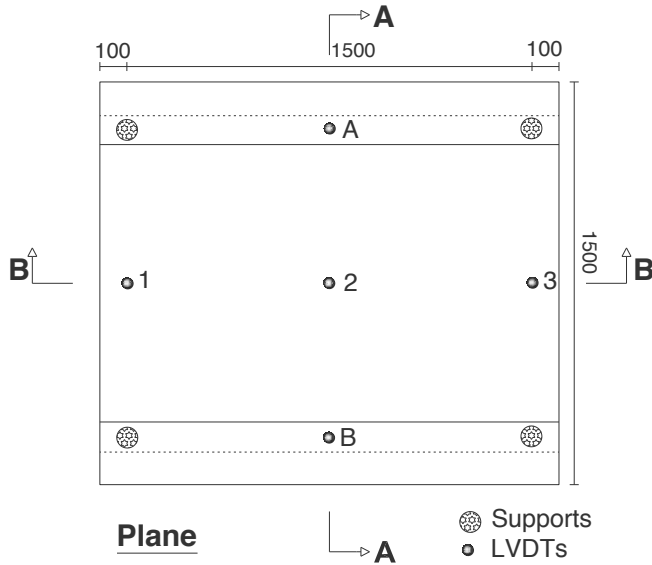


Figure 3 – Test setup, top view, in [mm].

Material properties

The targeted concrete quality was C30/37, and tested average concrete compressive strengths were 39 MPa and 43 MPa for the unstrengthened and strengthened specimen, respectively. Corresponding average concrete tensile strengths for the unstrengthened and strengthened specimen were 2.7 MPa and 3.1 MPa, respectively. Concrete strength was tested using six 150 mm cubes, and concrete compressive-, f_c , and tensile strength, f_t , were calculated using empirical relationships between these quantities and the cubes' measured cube-, f_{cu} , and splitting strengths, $f_{t,sp}$. The concrete strengths are summarized in Table 1.

Table 1. Concrete quality based on measured cube- and splitting strength.

	Compressive strength	Standard deviation	Tensile strength	Standard deviation
	f_c [MPa]	[MPa]	f_t [MPa]	[MPa]
B1	39	0.46	2.7	0.13
B2	43	0.52	3.1	0.22

Post tensioning

One specimen was strengthened with three straight seven wire prestressing strands, located at the longitudinal mid-section of the slab and at a distance of 375 mm on each side of the mid-section. The vertical locations of the tendons were at the center of the slab height, 55 mm from the bottom.

The diameter of the prestressing strands was 9.6 mm and the average tensile strength, f_{pu} , was 1860 MPa. Prestressing was conducted by hydraulic jacks and the effective prestress, f_{pe} , was 744 MPa or approximately $0.4f_{pu}$. The prestressing force was monitored by load cells at each tendon and the post tensioning procedure was a stepwise prestressing of one tendon at the time, starting with the central tendon and followed by the outer tendons.

Rectangular steel plates (110 x 120 x 15 mm) were used as anchor plates, transferring the stresses from the tendons, through the wedge anchors to the concrete structure, see Figure 4.



Figure 4 – Wedge anchor, load cell and anchor plate.

Loading and monitoring

Both specimens were subjected to two monotonic, deformation controlled line loads, as shown in Figure 2. Loading was conducted by a deformation controlled hydraulic jack until failure at a constant deformation rate of 0.01 mm/s, and the load was distributed by one transverse steel beam on top of two longitudinal steel beams as seen in Figure 2. The reason for choosing two line loads instead of a uniform load, which is the actual case caused by the ballast, was to obtain a zone with constant shear force between the load and the main beam.

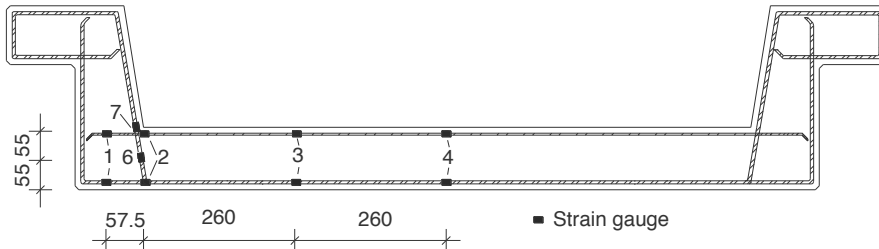


Figure 5 – Strain gauges on internal reinforcement, in [mm].

Displacements, rotation and global curvature were monitored by linear variable differential transducers (LVDTs), see Figure 3. Electrical resistance strain gauges measured the strains in the internal steel reinforcement, see Figure 5, and the load in the prestressing system was monitored by load cells, see Figure 4.

2.3 Shear design

The shear capacity was calculated according to beam theory in two design codes;

- The European design code EC2, [6]
- The Swedish design code BBK 04, [7]

BBK is based on the addition principle, where the total shear resistance, V_R , is calculated as the sum of the shear strengths of concrete, V_C , the shear reinforcement, V_S , and the prestressing V_P .

$$V_R = V_C + V_S + V_P \quad (1)$$

In order to provide a safe structure, the total shear resistance, V_R , must be greater than the shear forces, V_E , resulting from all loads acting on the structure as shown in equation (1).

$$V_R > V_E \quad (2)$$

EC2 has a slightly different approach. If the specimen contains shear reinforcement, the resistance of the concrete is neglected and the shear capacity is given as the resistance of the stirrups. In the case of no shear reinforcement, the shear resistance is given as the resistance of concrete where potential prestressing is included.

The test specimens in this report had no shear reinforcement, meaning that the shear strength was governed by the shear capacity of concrete and the contribution from prestressing. The design calculations are shortly described in the following sections and for detailed calculations the reader is referred to [8].

EC2

The general procedure for shear design of concrete structures is presented in chapter 6.2 of EC2. The design value for the shear resistance is given by equation (3).

$$V_{Rd,c} = \left[C_{Rd,c} \cdot k \cdot (100 \cdot \rho_l \cdot f_{ck})^{1/3} + k_1 \cdot \sigma_{cp} \right] \cdot b_w \cdot d \quad (3)$$

with a minimum of:

$$V_{Rd,c} = (v_{\min} + k_1 \cdot \sigma_{cp}) \cdot b_w \cdot d \quad (4)$$

As seen in equation (3), the shear capacity contribution, provided by the prestress is included in the shear capacity of the concrete. But the prestress can easily be separated into equation (5).

$$V_{Rd,c-prestress} = (k_1 \cdot \sigma_{cp}) \cdot b_w \cdot d \quad (5)$$

The values for k , k_1 , $C_{Rd,c}$ and v_{\min} can be found in the National Annex for each country, but the recommended values are

$$k = 1 + \sqrt{\frac{200}{d}} \leq 2.0 \quad (6)$$

$$k_1 = 0.15 \quad (7)$$

$$C_{Rd,c} = \frac{0.18}{\gamma_c} \quad (8)$$

$$v_{\min} = 0.035 \cdot k^{3/2} \cdot f_{ck}^{1/2} \quad (9)$$

Where

γ_c is the partial factor, which can be chosen as 1.2 or 1.5, depending on the design situation.

f_{ck} is the characteristic compressive cylinder strength of concrete at 28 days.

b_w is the smallest width of the cross-section in the tensile area.

d is the effective depth of a cross-section.

$$\rho_t = \frac{A_{st}}{b_w \cdot d} \leq 0.02 \quad (10)$$

A_{st} is the area of the tensile reinforcement, which extends $\geq (l_{bd} + d)$ beyond the section considered.

The stress, caused by prestressing is

$$\sigma_{cp} = \frac{N_{Ed}}{A_c} < 0.2f_{cd} \text{ [MPa]} \quad (11)$$

where

N_{Ed} is the axial force in the cross section due to loading or prestressing.

A_c is the area of the concrete cross section.

BBK

The general procedure for shear design of concrete structures is presented in chapter 3.7 of BBK 04. The design value for the shear resistance is given by the following equation.

$$V_R = V_C + V_S + V_P \quad (12)$$

The shear resistance of the concrete is calculated as

$$V_C = b_w \cdot d \cdot f_v \quad (13)$$

where

b_w is the smallest web width in the region of the effective height of a cross section.

d is the effective height of a cross section.

f_v is the formal shear strength of concrete.

The formal shear strength of concrete is calculated as

$$f_v = 0.30 \cdot \xi \cdot (1 + 50 \cdot \rho) \cdot f_{ct} \quad (14)$$

where

$$\xi = \begin{cases} 1.4 & \text{for } d \leq 0.2\text{m} \\ 1.6 - d & \text{for } 0.2\text{m} \leq d \leq 0.5\text{m} \\ 1.3 - 0.4d & \text{for } 0.5\text{m} \leq d \leq 1.0\text{m} \\ 0.9 & \text{for } 1.0\text{m} \leq d \end{cases} \quad (15)$$

$$\rho = \frac{A_{s0}}{b_w \cdot d} \leq 0.02 \quad (16)$$

f_{ct} is the design value for the tensile strength of concrete.

A_{s0} is the smallest area of the flexural tensile reinforcement in the zone between for maximum moment and zero moment.

The shear resistance of the prestressing can be calculated as

$$V_P = \frac{V_d}{1.2 \cdot \gamma_n} \cdot \left(\frac{M_0}{M_d} \right)_{\min} \quad (17)$$

where

M_d is the flexural moment caused by external loads.

M_0 is the moment which combined with the tensile force, causes zero strains.

γ_n is a safety factor.

The shear resistance of the concrete and the prestressing is limited to

$$V_C + V_P \leq b_w \cdot d \cdot (f_{ct} + 0.3\sigma_{cm}) \quad (18)$$

where

σ_{cm} is the average compressive stress in the uncracked cross-section, caused by effective tensile force or normal force, divided by $1.2 \cdot \gamma_n \cdot A$.

2.4 Flexural capacity

The flexural capacity of the cross-section shown in Figure 6 below is determined by defining the equilibrium equation (19).

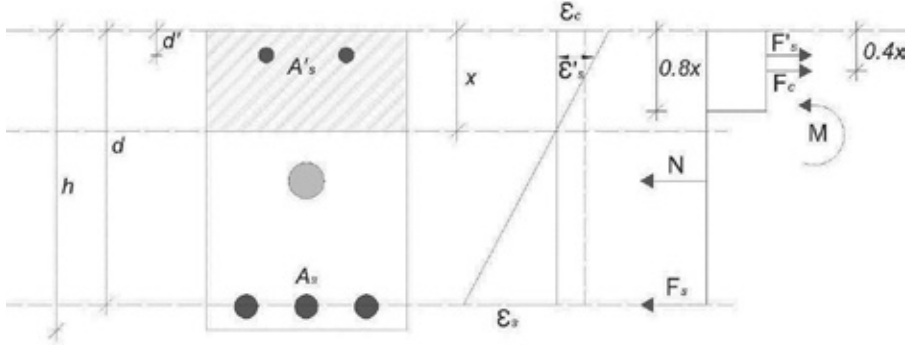


Figure 6 - Forces acting on a prestressed cross section.

By incorporating Hooke's law and assuming yielding in the tensile reinforcement at ULS, the horizontal equilibrium equation in the ultimate limit state will be

$$f_{cc} \cdot 0.8x \cdot b + \varepsilon'_s E_S \cdot A'_s - N - f_{st} \cdot A_S = 0 \quad (19)$$

where

- f_{cc} is the compressive stress of concrete.
- b is the width of the cross section.
- ε'_s is the strain in the compressive reinforcement.
- E_S is the elastic modulus for steel.
- A'_s is the area of the compressive steel.
- N is the prestress.
- f_{st} is the yield strength of the tensile reinforcement.
- A_S is the area of the tensile reinforcement.

The distance to the neutral layer, x , can be solved with the following equation

$$x = \frac{-C_2}{C_1} \quad (20)$$

where

$$\left. \begin{aligned} C_1 &= 0.8 \cdot f_{cc} \cdot b \\ C_2 &= \varepsilon'_s E_S \cdot A'_s - N - f_{st} \cdot A_S \end{aligned} \right\} \quad (21)$$

Through moment equilibrium around the concrete resultant force, F_C , which is assumed to be located at a distance of $0.4x$ from the concrete's top fiber at ultimate limit state, the flexural capacity can be expressed as

$$M = f_{st} \cdot A_S (d - 0.4x) + N \left(\frac{h}{2} - 0.4x \right) - \varepsilon'_s E_S \cdot A'_s (d'_s - 0.4x) \quad (22)$$

For a cross section without prestress, the flexural capacity is determined by setting the prestressing force, N , to zero in Equation (19) – (22).

3. RESULTS

The failure load, P_{max} , was 344 kN and 380 kN for the unstrengthened and strengthened specimen, respectively, and both specimen failed in flexure. The maximum load, P , that corresponds to the shear capacity calculated according to EC2 and BBK are given in Table 2. M_{cap} is the maximum load, P , corresponding to the flexural capacity.

Table 2 – Load, P , required to reach calculated shear capacity (according to EC2 and BBK), flexural capacity, M_{cap} , and tested failure loads, P_{max} . All capacities are calculated for the entire cross section.

	EC2	BBK	M_{cap}	P_{max}
	[kN]	[kN]	[kN]	[kN]
B1	258	308	294	344
B2	286	322	356	380

3.1 Deformation

When the specimens were subjected to loading, the main beams rotated inwards against the trough and the slab deflected, as illustrated in Figure 7. The measured inwards rotations of the main beams and deflection at mid span are presented in Figure 8 and 9, respectively.

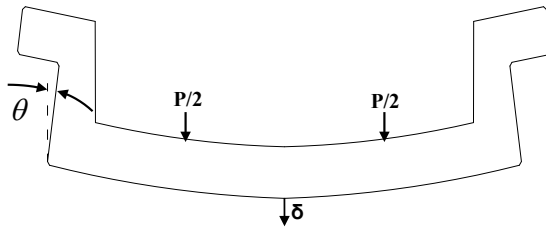


Figure 7 – Rotation and deflection of specimen.

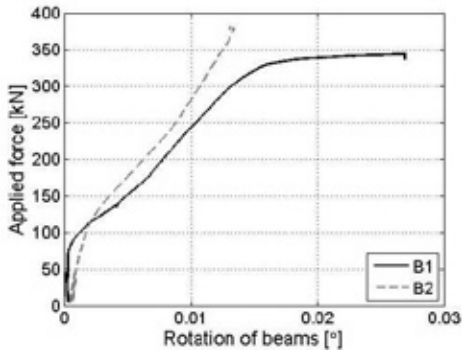


Figure 8 - Rotation of main beams.

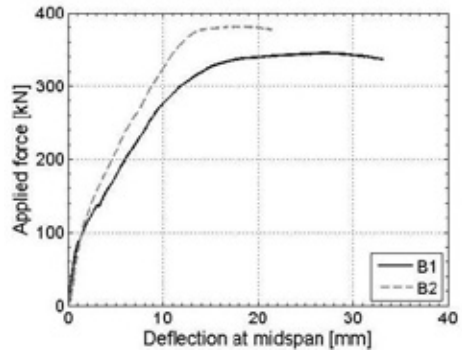


Figure 9 - Deflection at midspan.

A curvature rig was used to monitor the global curvature and the outcome is presented in Figure 10. Local curvature, Figure 11, is calculated from the strains in the internal reinforcement, equations are described in [9]. The main difference between global and local curvature is the section considered. While the global curvature is the average curvature for the structure, the local curvature presents the curvature in one vertical section of the structure and requires two strain gauges in the vertical line.

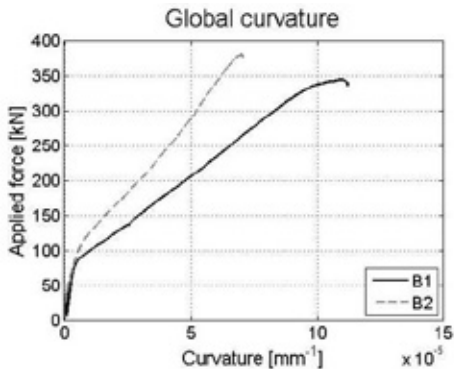


Figure 10 - Global curvature.

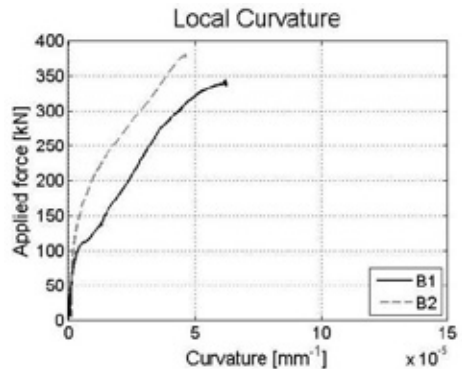


Figure 11 - Local curvature.

3.2 Strains

Figure 12 presents the strain curves for transversal tensile reinforcement at the center point of the test specimen, according to Figure 5, and the corresponding strain curves for compressive reinforcement is presented in Figure 13. The tensile- and compressive reinforcement had diameters of 8 and 6 mm, respectively. Reinforcement grade was B500B, with a strain at yielding of approximately $2500 \mu\text{m/m}$. Since the prestressing force is causing compression of the tensile reinforcement before loading starts, B2 initially has a small negative value.

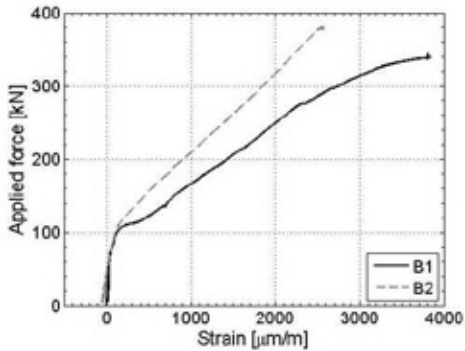


Figure 12 - Strain in tensile reinforcement.

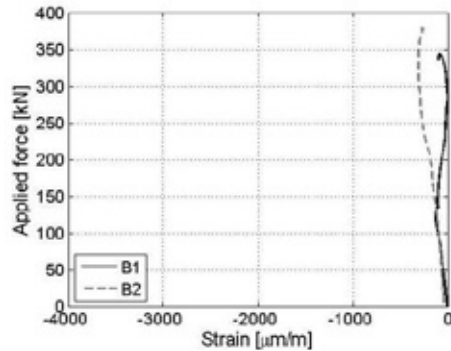


Figure 13 - Strain in compressive reinforcement.

Strains were measured in bent up reinforcement bars, with a diameter of 8 mm, at the junction of the slab and the main girders, see strain gauge nr. 6 in Figure 5. Figure 14 presents the strain readings from the bent up reinforcement at mid height of the slab.

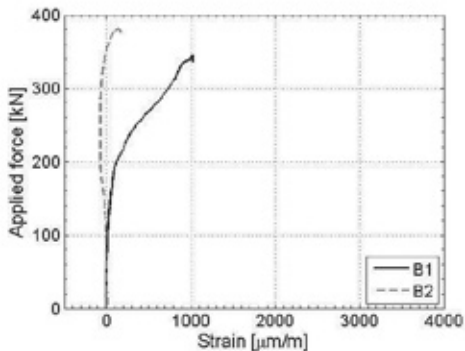


Figure 14 - Strain in bent up reinforcement.

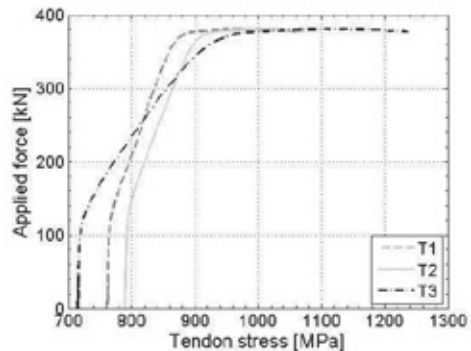


Figure 15 – Tendon stresses.

The tendon forces in specimen B2 were measured by load cells and the calculated stresses are presented in Figure 15, where T2 represents the central tendon. The tensile strength of the tendons was 1860 MPa.

4. ANALYSIS AND DISCUSSION

Transversal post tensioning has a positive effect on the behavior of concrete trough bridges as seen in the laboratory test results presented in Figure 8 – 15. The deformations are clearly reduced in terms of decreased vertical displacements of the slabs and less rotation of the main girders. In an in-situ situation, when the trough is filled with ballast, loading will force the main beams to rotate inwards, but the rotation will be prohibited by the ballast inside of the trough. Instead of rotating the beams, the loading will create torsion at the junction of the slab and the main girders. The effect of prestressing is decreased rotation of the main girders, as seen in Figure 8.

Figure 12 shows that the strain levels in the tensile reinforcement are also significantly decreased after prestressing, which should render in an increased flexural capacity. The calculations given in section 2.3 also indicated an increased flexural capacity, see Table 2.

The main objective of the laboratory tests was to investigate how the prestressing affected the transversal shear behaviour and if the capacity of the slab could be increased. The largest shear forces, in the current test setup, appeared in the exterior side of the line loads, i.e. between line load and beam, see Figure 2. Since there was no shear reinforcement in the slab, the shear stresses were best represented by the strain levels in the bent up reinforcement at the junction of the slab and the main girders as seen in Figure 5. The strains in the bent up bars were dramatically affected by post-tensioning, i.e. the strain was significantly smaller in the strengthened specimen. The post tensioned specimen also exhibited compression before any tension could be detected in the bent up bars. The reduced strains in the bent up bars, for the strengthened specimen, indicate a relief in shear stress and thus an increase in the shear capacity.

The tendons were prestressed up to an effective prestress of about 40% of the tendon capacity, generating a total prestressing force of 124 kN for the three tendons. It would therefore be possible to increase the prestressing force, which could result in an even larger capacity increase. Figure 16 illustrates how the load capacities, calculated from the shear capacities according to EC2 and BBK, are affected by increasing the prestress.

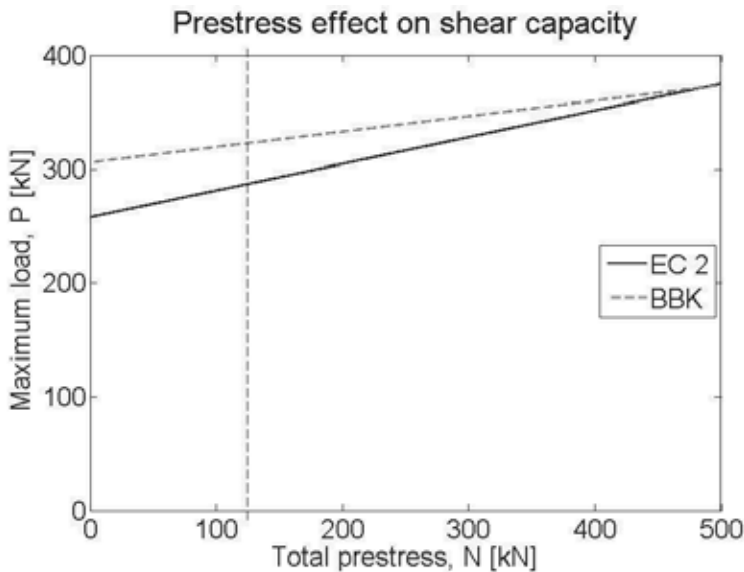


Figure 16 – Effect of increasing the prestress.

EC2 and BBK starts with load capacities of 258 and 308 kN, respectively for an unstrengthened specimen. For a prestress of 124 kN (dashed horizontal line in Figure 16), the load capacities has increased up to 286 and 322 kN for EC2 and BBK, respectively. As seen in Figure 16, the prestress impact on shear capacity is higher for EC2, i.e. the slope of the solid line is steeper. When the total prestress approaches 500 kN, the shear capacity according to BBK and EC2 coincides at approximately 375 kN.

Both specimens failed in flexure, in contrast to the design calculations summarized in Table 2. According to EC2, the specimen would have failed in shear and calculations according to the Swedish concrete design code, BBK, indicated that the unstrengthened specimen would fail in flexure and the strengthened one would fail in shear. The two design codes, however, underestimates the shear capacity and the significant decrease of strains in the bent up reinforcement for B2, as seen in Figure 14, indicates an underestimation of the strengthening effect as well.

The actual test setup with a trough bridge located on top of four point supports, loaded with two line loads, was obtained by having two steel beams on top of the concrete slab. Different stiffness's of the steel beams and the concrete slab would theoretically result in different flexural behavior and masonite strips and plaster were therefore introduced as an intermediate layer. The desired function of the intermediate layer was to obtain uniform loading along the entire line loads, and the spherical supports also had similar function. Although no space could be detected between the steel beams and the concrete slab during loading, a fully uniform line load cannot be guaranteed.

By using scaled down specimens, size effects are affecting the correspondence of the test results to real size trough bridges, see e.g. [10]. Aggregate size and interlocking, as well as reinforcement design and dimensions are affecting the shear capacity, but size effects are not analyzed in this paper.

5. CONCLUSION

The laboratory tests indicate that post-tensioning is a method which should be possible to be used for strengthening of concrete trough bridges in shear (and flexure). For the strengthening part, there are hydraulic jacks designed for prestressing of steel strands and bars. This procedure does not require any electricity or heavy machinery, just a hydraulic jack and a pump, which means this can be performed at most remote locations. One part of the strengthening procedure though, which was not included in this laboratory investigation, is the drilling of holes through the structure in which the prestressing cables or bars are inserted. This has however been performed earlier in [11].

Transversal post-tensioning increases both the shear capacity and the flexural capacity, which is confirmed in design calculations as well as laboratory tests. The laboratory tests, however, indicate that both EC2 and BBK are restrictive in estimating the strengthening effects of post-tensioning.

6. FUTURE RESEARCH

Transversal post-tensioning is an appropriate method for increasing the shear capacity of reinforced concrete trough bridges. The method will be tested on a real trough bridge in the summer of 2012.

Further laboratory tests are also required to confirm the results from this report and for investigating the effect of changing the distance between tendons and changing the prestress.

The technique for drilling holes through the bottom slab needs to be investigated further, in order to develop an effective procedure with high precision.

A rail transportation project called MAINLINE, [12], recently started in Europe, with the aim to develop new renewal interventions and maintenance strategies. Another aim is to develop tools to inform decision makers about the economic and environmental consequences of different maintenance and renewal intervention options being considered. MAINLINE proposes that these new methods will render in annual savings of at least 300 M€ across Europe with a reduced environmental footprint in terms of embodied carbon and other environmental benefits.

ACKNOWLEDGEMENTS

The Swedish transport agency Trafikverket is acknowledged for funding the research project. The laboratory tests have been performed in cooperation with Complab, at Luleå University of Technology, and the staff has been most helpful in performing the tests.

REFERENCES

1. Bell, B., (2004), "*D1.2 European Railway Bridge Demography*", European FP 6 Integrated project "Sustainable Bridges", Assessment for Future Traffic Demands and Longer Lives, <http://www.sustainablebridges.net>, accessed date 10 January 2012.
2. Sas, G., Blanksvärd, T., Elfgren, L., Enochsson, O. and Täljsten, B., (2012), "*Photographic strain monitoring during full scale failure testing of Örnköldsvik Bridge*", Journal of Structural Health Monitoring, Vol. 11, No. 4, July 2012, pp. 489-498.
3. Sustainable bridges, (2008), "*Sustainable Bridges – Assessment for Future Traffic Demands and Longer Lives*", A European Integrated Research Project during 2003-2008. Four guidelines and 35 background documents are available at <http://www.sustainablebridges.net>.
4. Enochsson, O., Nordin, H., Täljsten, B., Carolin, A., Kerrouche, A., Norling, O., Falldén, C., (2007), "*Field test – Strengthening of the Örnköldsviks Bridge with near surface mounted CFRP rods*", deliverable D6.3 within Sustainable Bridges, 55 p.
5. Bergström, M., Danielsson, G., Johansson, H. & Täljsten, B. (2004), "*Mätning på järnvägsbro över Fröviån*", Technical Report, Luleå University of Technology, Luleå, Sweden, 73 p.
6. CEN, (2008), "*EN 1992-1-1:2004 Eurocode 2: Design of concrete structures - Part 1-1: General rules and rules for buildings*", CEN: European Committee for Standardization, Brussels (Belgium).
7. Boverket, (2004), "*Boverkets handbok om betongkonstruktioner: BBK 04*", 3rd edition, Boverket, Karlskrona (Sweden), ISBN 91-7147-816-7.
8. Nilimaa, J., (2012), "*Upgrading of Reinforced Concrete Trough bridges – Laboratory Tests*", Technical Report, Luleå University of Technology, Luleå, Sweden.
9. Bergström, M., (2009), "*Assessment of Existing Concrete Bridges: Bending Stiffness as a Performance Indicator*", Doctoral Thesis, Luleå University of Technology, March 2009, 241 p.
10. Bazant, Z. P. & Kim, J-K., (1984), "*Size effect in shear failure of longitudinally reinforced beams*", Journal of the American Concrete Institute, Vol. 81, No. 5, September 1984, pp. 456-468.
11. Bennitz, A., Täljsten, B. and Danielsson, G., (2012), "*CFRP strengthening of a railway concrete trough bridge – a case study*", Structure and Infrastructure Engineering, Vol. 8, No. 9, September 2012, pp. 801-816.

12. MAINLINE, (2011), "*A European Community 7th Framework Program research project with the full title: MAINtenance, renewaL and Improvement of rail transport iNfrastructure to reduce Economic and environmental impacts*", Research Project 2011-2014 with 19 partners, information available at <http://www.mainline-project.eu>.

Nordic Workshop on Finite Element Analysis of Concrete Structures



Mikael Hallgren
Adj. Professor, PhD
Tyréns AB
Peter Myndes Backe 16
SE-118 86 Stockholm
mikael.hallgren@tyrens.se

ABSTRACT

A Nordic workshop on finite element analysis of concrete structures was held at Chalmers University of Technology on October 13, 2011. Participants from universities as well as practising structural engineers were invited. 18 presentations were given and a wide range of issues from basic research on the subject to practical applications were covered. The present paper gives a summary of the workshop.

Key words: Workshop, Finite Element Method (FEM), Finite Element Analyses (FEA), Reinforced Concrete (RC) Structures.

1. INTRODUCTION

Since 1975, the Research Committee of the Nordic Concrete Federation has promoted Nordic workshops or mini-seminars within the field of concrete research. As the research on and the use of numerical modelling of reinforced concrete structures with the finite element method (FEM) has increased rapidly over the last years, it was time to arrange a Nordic workshop on this topic.

The workshop was held on October 13, 2011, at Chalmers University of Technology. About 35 researchers and structural engineers participated. The participants came from Sweden, Norway, Finland and the Netherland. In total, 18 presentations were given. The presentations covered three main subjects; Research, Practical application in design and assessment, and Guidelines. All presentations can be found on the website of the Swedish Concrete Association [1]. A short summary of each presentation will be given in the following.

2. RESEARCH

Karin Lundgren from Chalmers started the workshop by giving an overview of the research on FEA of concrete structures performed at Chalmers since the late 1980ies. The research has comprised fundamental material modelling, columns, modelling of whole bridges, bond and anchorage, deteriorated structures, impact loading and safety methods. Some challenges and possible areas of further research are new materials such as textile reinforcement, time effects on deteriorated structures, optimisation of structures by FEA and multi scale modelling.

Annette Jansson from Färdig Betong presented the modelling of tie element tests and gave reflections on the results. Tie elements without and with various contents of steel fibres were tested in tension. All elements were centrally reinforced by one bar. The tests were then modelled and simulated by non-linear finite element analysis (NLFEA). Good conformity between tests and NLFEA was achieved. However, surprisingly the FE models with coarse mesh gave better results than the dense FE models. The reason was discussed at the workshop and the stiffening effect of a very dense mesh, as in this case, was mentioned as a possible explanation.

David Fall from Chalmers presented the NLFE modelling of steel fibre reinforced concrete beams subjected to four-point bending in previous tests. The beams were also lightly reinforced with rebars. The fibres increased the flexural capacity and this could also be reasonably well simulated in the NLFEA. The NLFEA were used to explain the reason for the increase and the mechanical mechanisms.

Mathias Flansbjerg from SP presented a detailed study of the cracking process at shear failure of RC beams. The aim of the investigation is to capture factors affecting the shear cracking and failure process. The research method is microscopical analysis in combination with 3D Digital Image Correlation (DIC), Acoustic Emission (AE) and NLFEA. Hereby it is possible to determine on what stage the cracks have been formed and their relation to the micro and meso structure. The combination of methods will increase the understanding of shear failures.

Kamyab Zandi Hanjari from CBI presented his research project on the analysis of large corrosion penetrations. RC specimens with corrode rebars were subjected to eccentric pull-out tests which were later simulated by 3D NLFEA, including the corrosion phase with an extended corrosion model and the mechanical pull-out tests. The rust flowing through the cracks gave a favourable effect. The modelling gave good correspondence with the test results for low corrosion attacks and the extended corrosion model gave a qualitatively reasonable response.

Filip Nilenius from Chalmers presented a project on multiscale modelling of coupled chloride-moisture diffusion in concrete. In two coupled 2D FEA, the concrete is first considered heterogeneous in the mesoscale and then homogeneous in the macroscale while subjected to time evolution of moisture and chlorides. Hereby, the material heterogeneities are accounted for, including randomness and with reduced need for empirical models.

Max Hendriks from TU Delft showed the method of Sequentially Linear Analysis (SLA) as an alternative to incremental- iterative methods such as the Newton-Raphson method, which is widely used in NLFEA. The structural response is captured through a series of scaled linear analysis to identified critical points on the load-deflection curve. SLA is a relatively simple but effective and robust NLFEA technique which is especially suited for brittle structural behaviour.

Mario Plos from Chalmers presented a new safety format for NLFEA. The partial factor method commonly used in design is not adequate in NLFEA as it may result in the wrong failure mode. A global safety format is needed. The Eurocode 2 and the new Model Code 2010 give some methods for this. However, the modelling uncertainty is not accounted for in these methods. The proposed, new safety format includes modelling, geometrical and material uncertainties.

Morgan Johansson from Reinertsen presented some results from four master thesis projects on concrete cracking due to restraining forces. In all theses, NLFEA has been used as a tool. The first two theses dealt with tie rods and the question of minimum reinforcement for crack control.

Critical parameters were identified and it was concluded that the approach in some codes could be non-conservative. The third thesis dealt with crack control in edge beams. Here, a concept for simplified design was proposed. The fourth thesis dealt with crack control in walls. By modelling and analysing different reinforcement configurations, some more efficient placing of reinforcement could be proposed.

Folke Höst from Tyréns presented a research project where NLFEA is used for assessment of historical masonry structures. The aim is to increase the use of ruins by secured masonry and comfortable climate. The concrete damaged plasticity material model in Abaqus Standard is used in the NLFEA. However, the most important parameter is the geometry of the structures. The structures are modelled by importing the results from software which interprets point clouds from laser scanning. The development of the application includes risk assessment, identification of damage cause, analysis of previous poor strengthening and assessment of structural changes.

3. PRACTICAL APPLICATION IN DESIGN AND ASSESSMENT

Daniel Eriksson and Tobias Gasch from Vattenfall Engineering presented their Master thesis on FEA of anchorage to concrete. The application is in nuclear facilities where several thousands of anchor plates can be found in each nuclear power plant. Due to the required power uprate, the anchor plates will be subjected to new load. Different types of anchors were simulated with NLFEA in order to check the design and to simplify the future design process.

Mikael Hallgren from Tyréns presented some examples of assessment of existing RC structures and design check of new RC structures using NLFEA. What previously was a tool only used in research is now available for the engineering practice. Modern codes like the Eurocode and the Model Code open up for the use of NLFEA. However, the material models usually have many parameters and most of them are not covered by the codes. Satisfying global safety formats that cover all types of uncertainties are still not available in the codes. Good practice is to check the results from the advanced analysis with simple models and hand calculations.

Helén Broo from Skanska presented applications of FEA in the structural design of a roundabout bridge within the road project E45 Bohus. The structure is highly non-uniform and without any natural symmetries. A global FE model was loaded with design loads. The linear elastic analysis gave sectional forces for the design of reinforcement. The model was also used for design of the various construction stages. The piers and foundations were designed with local FE models.

Dan-Evert Brekke and Espen Aas Smedsrud from Multiconsult presented some experience of FEA and design of concrete structures using ANSYS and Multicon. The structures are generally modelled with plate and shell element and in some cases with solid elements. The sectional forces resulting from the FEA for each load case are converted to a database of the design program Multicon. By combining results from the database for each design combination, the input to various design modules is given and design with non-linear sectional analysis is performed. The method has successfully been used in the design of off-shore structures as GBS of oil platforms and on-shore structures such as bridges.

Azmi Al-Eesa presented some experience and gave comments on the use of the commercial FE software FEM-Design by StruSoft. The program has three modules included; modelling, analysis and design. The models can be imported by dwg and dxf files. Design can be performed

by 10 different national standards, including Eurocode. Some advantages and god features as well as problems and features that need to be further developed were presented and discussed.

Richard Malm from KTH and Vattenfall presented simulations of crack propagation in concrete hydropower dam structures. Several larger dams in Sweden have been found to be cracked due to thermal deformations. NLFEA have been used to explain the cause of the cracks. The influence of distribution of material properties on the crack trajectory has been studied. Preliminary results show a difference in the trajectory obtained from deterministic analysis with mean values compared to the most probable crack trajectory obtained from probabilistic analyses.

4. GUIDELINES

Ane de Boer from the Centre for Infrastructure in the Netherlands presented the work on a guideline for NLFEA of prestressed and reinforced concrete beams. As new codes like the Eurocode 2 and the ModelCode 2010 include the possibility of NLFEA and because computers now have faster CPU, the use of NLFEA has increased and a guidelines is needed. The Dutch guideline includes recommendation for safety format, specific input properties for material models, finite elements (type and size), load and support models, load increments and convergence limits, and also gives checklists on what has to be included in the analysis report. A validation of the guideline has been performed and shows that the recommended calculation process is robust.

Mario Plos from Chalmers presented a joint project between KTH, Chalmers and Trafikverket (Swedish Transport Administration) in which a handbook for finite element analysis of structures is developed. The background is that FEA is increasingly used in practice and that Trafikverket requires 3D analysis in bridge design. The handbook includes general recommendations for design and analysis with FEM and guidelines for FE modelling. Furthermore, the handbook covers static and dynamic linear FEA and NLFEA considering both geometrical and physical non-linearity as well as solution methods and convergence. The handbook considers both steel and concrete structures.

5. CONCLUDING REMARK

The workshop showed that FEA and NLFEA of concrete structures no longer are tools for research only. Many of the presentations gave examples where these advanced tools are used for practical engineering and for applied development. Guidelines and handbooks are developed to help the engineers in the use. However, for research purpose NLFEA still has a tremendous impact on the efforts to understand complicated mechanisms in plain and reinforced concrete structures.

REFERENCE

1. Pdf-files of the Power Point presentations given at the Nordic Workshop on FEA of concrete structures, October 13, 2011, at Chalmers University of Technology:
<http://betongföreningen.se/2011/10/temp-nordic-workshop/>

Research Council and Editorial Board for Nordic Concrete Research

Prof. Dr. Olafur H. Wallevik, Chairman for the Research Committee

Dr. Dirch H. Bager, Editor of Nordic Concrete Research

**Danish
Concrete
Association**

Dr. Dirch H. Bager
DHB-Consult
Lavendelparken 5
DK - 9310 Vodskov
Tel: +45 98292412
Mobile: +45 2049 7324
E-mail: dirch.bager@bbnpost.dk

Mr. Claus Pade
Concrete Centre,
Danish Technological Institute
Gregersensvej
DK - 2630 Taastrup
Tel: + 45 7220 2183
E-mail: cpa@teknologisk.dk

**Finnish
Concrete
Association**

Mr. Juha Valjus
Concrete Association of Finland
Unioninkatu 14 PL 381
FI - 00131 Helsinki
Tel: +358 41 533 6020
Mobile: +358
E-mail: juha.valjus@betoniyhdistys.fi

Lic.Sc.Tech. Klaus Juvas
Consolis Technology
Box 72
FI - 21291 Rusko
Mobile: +358 40 5160 316
E-mail: klaus.juvas@consolis.com

**Icelandic
Concrete
Association**

Prof. Dr. Olafur H. Wallevik
Innovation Center Iceland
IS - 112 Keldnaholti
Tel: +354 522 9000
Mobile: +354
E-mail: wallevik@ru.is

**Norwegian
Concrete
Association**

Dr. Terje F. Ronning
Norcem, FoU Department
P.O.Box 38
N - 3991 Brevik
Tel.: +47 3557 2347
Mobile: +47 9157 6046
E-mail: terje.ronning@norcem.no

Dr. Ing. Helge Brå
Norwegian Public Road Authority
Abelsgate 5
N - 7030 Trondheim
Mobile: +47 9709 5277
E-mail: helge.braa@vegvesen.no

**Swedish
Concrete
Association**

Adjunct. Prof., Tekn. Dr. Mikael Hallgren
Tyréns AB
Peter Myndes Backe 16
SE - 118 86 Stockholm
Tel: +46 104 522 351
Mobile: +46 70 661 05 33
E-mail: Mikael.Hallgren@tyrens.se

Tekn. Dr. Peter Utgenannt
CBI Swedish Cement and Concrete Research
Institute
P.O. Box 857
SE - 501 15 Borås
Tel: +46 105 166 870
Mobile: +46 706 452 008
E-mail: peter.utgenannt@cbi.se

05 December 2012

Active reviewers for Nordic Concrete Research as per December 2012**DENMARK**

Dr. Dirch H. Bager
 Prof., Dr. Lars Damkilde
 Dr. Mette Glavind
 Prof., Dr. Per Goltermann
 Mr. Oscar Klinghoffér
 Prof., Dr. John Forbes Olesen
 Mr. Claus Pade
 Prof., Dr. Eigil V. Sørensen
 Prof., Dr. Jens Peder Ulfkjær

FINLAND

Dr. Klaus Juvas
 Dr. Matti V. Leskala
 Prof., Dr. Jussi Mattila
 Mr. Erik Nordenswan
 Dr. Jouni Punkki
 Mr. Juha Valjus

ICELAND

Mr. Einar Einarsson
 Mr. Haukur J. Eiriksson
 Dr. Gisli Gudmundsson
 Mr. Karsten Iversen
 Mr. Torfi G. Sigurdsson
 Mr. Sveinbjörn Sveinbjörnsson
 Dr. Jon E. Wallevik
 Prof., Dr. Ólafur H. Wallevik
 Prof., Dr. Børge J. Wigum

NORWAY

Dr. Helge Brå
 Ms. Danielle Bosnjak
 Mr. Anton Gjørven
 Mr. Steinar Helland
 Dr. Bernt Jacobsen
 Prof., Dr. Terje Kanstad
 Dr. Terje F. Rønning
 Mr. Tor Kristian Sandaker
 Mr. Sverre Smeplass
 Mr. Hans Stemland

SWEDEN

Prof., Dr. Anders Ansell
 Dr. Thomas Blanksvärd
 Prof. Lennart Elfgren
 Prof., Dr. Mats Emborg
 Prof., Dr. Kent Gylltoft
 Prof., Dr. Mikael Hallgren
 Prof., Dr. Jan-Erik Jonasson
 Prof., Dr. Björn Lagerblad
 Prof., Dr. Karin Lundgren
 Prof., Dr. Tang Luping
 Prof., Dr. Per-Erik Petersson
 Prof., Dr. Johan Silfwerbrand
 Dr. Peter Simonsson
 Dr. Peter Utgenannt

